Intersubband surface plasmon polaritons in all-semiconductor planar plasmonic resonators

M. Załużny

Institute of Physics M. Curie-Skłodowska University, Pl. M. Curie-Skłodowskiej 1, 20-031 Lublin, Poland

We theoretically discuss properties of intersubband surface plasmon polaritons (ISPPs) supported by the system consisting of a multiple quantum well (MQW) slab embedded into planar resonator with highly doped semiconducting claddings playing the role of cavity mirrors. Symmetric structures, where the MQW slab occupies the whole space between the claddings and asymmetric structures, where the MQW occupy only half of the space between mirrors, are considered. We focus mainly on the nearly degenerate structures where intersubband frequency is close to frequency of the surface plasmon of the mirrors. The ISPP characteristics are calculated numerically using a semiclassical approach based on the transfer matrix formalism and the effective-medium approximation. The claddings are described by the lossless Drude model. The possibility of engineering the dispersion of the ISPP branches is demonstrated. In particular, for certain parameters of the asymmetric structures we observe the formation of the multimode ISPP branches with two zero group velocity points. We show that the properties of the ISPP branches are reasonably well interpreted employing quasiparticle picture provided that the concept of the mode overlap factor is generalized, taking into account the dispersive character of the mirrors. In addition to this, we demonstrate that the lossless dispersion characteristics of the ISPP branches obtained in the paper are consistent with the angle-resolved reflection-absorption spectra of the GaAlAs-based realistic plasmonic resonators.

I. INTRODUCTION

Strong coupling between collective intersubband excitation in a multiple quantum well (MQW) structure and the ground photonic mode of the semiconductor microcavity (MC) leads to the formation of coherent mixed modes termed intersubband cavity polaritons. Such types of mode, named an upper polariton branch and lower polariton branch, were first observed in 2003 as a double-peak structure in the angle-resolved mid-IR absorption spectra of semiconductor MC with embedded MQW [1].

The intersubband cavity polaritons have attracted great attention of the research community. It is mainly due to the fact that intersubband optoelectronic devices operating in a strong coupling regime, i.e., when the coherent coupling overwhelms the dissipative processes, have potential for applications. For example, quantum cascade structures embedded in MC have been used to demonstrate electrically pumped light-emitting polaritonic devices in the mid-IR [2]. A road map for the development of intersubband polariton LED and laser has recently been suggested [3].

While the majority of work on the intersubband cavity polaritons has explored all dielectric, hybrid metal-dielectric, or double-metal [4–7] MCs, attention has also been paid to the resonators in which n-doped semiconductor layers play the role of mirrors (see, e.g., [8–10]). It is mainly connected with the fact that the presence of free carriers in semiconductor mirrors leads to the reduction of their dielectric function. Owing to that, such plasmonic mirrors can be substantially thinner compared to purely dielectric mirrors. Additionally, they allow for the electrical pumping of the intersubband polaritonic devices.

However, the presence of free electrons in the claddings leads to the formation of a new type transverse magnetic (TM) polarized surface plasmon polariton (SPP) modes. In the case of the resonator with identical semi-infinite metallic/plasmonic mirrors, theory predicts the formation of one symmetric SPP mode $S_{SPP}(\equiv TM_0)$ and one antisymmetric SPP mode $A_{SPP}(\equiv TM_1)$ [10–17]. We adopt the convention that the S_{SPP} and A_{SPP} modes are referred to as plasmonic-type modes while the higher TM modes supported by the resonator are treated as the photonic-type modes.

The essential difference between the photonic- and plasmonic-type modes is that plasmonic modes go asymptotically (always from a low-frequency side [18]) towards the surface plasmon frequency ($\omega_{p,\text{mirr}}^{\text{surf}}$) of the isolated interface as the in-plane wave vector $\mathbf{k}_\parallel$ approaches infinity. Moreover, the A_{SPP} mode, in contrast with the S_{SPP} mode, has nonzero cutoff frequency (ω_A^{cutoff}), i.e., the frequency at $k_\parallel = 0$. This frequency increases, up to the mirror plasma frequency ($\omega_{p,\text{mirr}}$), with the decreasing mirror separation (L_{MC}).

Owing to the above-mentioned flexibility of the A_{SPP} dispersion, Shin *et al.* [19] were able to design a metal-dielectric-metal MC whose resonance frequency was practically independent of the angle incidence of light and consequently of $k_\parallel$. Omnidirectional light emission via the A_{SPP} mode has also been reported [20,21].

It is obvious that when L_{MC} is small enough then $\omega_A^{\text{cutoff}} > \omega_{p,\text{mirr}}^{\text{surf}}$. It means that the formation of the backward (with the negative group velocity) and forward (with the positive group velocity) antisymmetric SPP branches becomes possible. Such branches have been observed experimentally in metallic [22] and all-semiconductor [23] structures. Moreover, Law *et al.* [24] have demonstrated all-semiconductor mid-IR plasmonic absorbers based on the resonant excitation of the negative group velocity branch. Recently, this branch has also been employed for frequency doubling of light in metallic waveguides [25].

In the lossless limit, the formation of the backward and forward propagating branches is associated with the appearance of the stopped-light mode, i.e., the mode with the zero group velocity (ZGV) [26,27]. However, Reza *et al.* [28] have shown, employing the complex-wave-vector picture, that the presence of intrinsic loss in plasmonic claddings dramatically changes the dispersion curves near slow-light regions. Fortunately, the problems associated with the losses can be partially overcome using, in contrast to the usual continuous-wave light, optical pulses whose duration is shorter than the surface plasmon decay [29,30]. In this way, the effects of losses can be loaded not into spatial domain but into the time domain. Simulations show that in the case of temporal losses, unlike the case of the spatial losses, the formation of the ZGV points (in the Re ω-$k_\parallel$ plane) is possible even in the presence of the realistic levels of dissipative loss [31]. It means that incident pulses, with a central frequency near the ZGV point, can be stopped in the sense that the center of the envelope does not drift over time [32]. It is worth stressing that the presence of the ZGV points provides a cavity-free feedback mechanism and, furthermore, has the potential to confine lasing modes on deeply subwavelength scale when gain is incorporated between plasmonic claddings [32,33].

As mentioned, properties of the A_{SPP} mode can be tuned to a large extent by changing L_{MC} or/and $\omega_{p,\mathrm{mirr}}$. Thus, the dispersion characteristics of the polariton branches, originating from the coupling of the A_{SPP} mode with electronic excitation, should be also substantially modified by changing the above-mentioned parameters. This suggestion is consistent with the results reported in Refs. [18,34–36] where the metallic resonators, uniformly filled with dielectric (cubic) material possessing an electronic resonance, are studied theoretically and experimentally, respectively. In particular, the authors of [18] show that the formation of the ZGV point (more precisely the minimum), in the dispersion curve of the exciton surface plasmon polariton branches originating from the A_{SPP} mode, is possible. Such a minimum may serve as an effective trap for exciton-polariton population at high nonresonant excitation of the structure.

In light of the above discussion, it is apparent that the possibility of the engineering of the dispersion of the intersubband-SPP (ISPP) branches, in plasmonic resonators, seems to be attractive from the viewpoint of intersubband polariton optoelectronics but also because of the inherent interest of their physical properties. However, in typical subwavelength double-metallic resonators with embedded MQW (see, e.g., [4,6]) mirror plasma frequency $\omega_{p,\mathrm{mirr}}$ (and consequently the surface plasmon frequency $\omega_{p,\mathrm{mirr}}^{\mathrm{surf}}$) is much larger than ω_{IT} (= the frequency of the collective intersubband excitation supported by isolated QW). Then, the resonant coupling of the intersubband excitation with the S_{SPP} mode is only possible in such structures. On the other hand, in the systems studied experimentally by Dupont *et al.* [8,9], the n-doped semiconductor layers (with $\omega_{p,\mathrm{mirr}} \ll \omega_{\mathrm{IT}}$) play the role of the mirrors. Consequently, intersubband excitation couples resonantly not with the plasmonic-type modes but only with the photonic-type modes located far above $\omega_{p,\mathrm{mirr}}$ [37,38]. Nevertheless, it is reasonable to expect that the systems with n^+-doped semiconductor mirrors can be designed so as to achieve an interesting situation when $\omega_{\mathrm{IT}} = \omega_{p,\mathrm{mirr}}^{\mathrm{surf}} \approx \omega_A^{\mathrm{cutoff}}$. It is obvi-
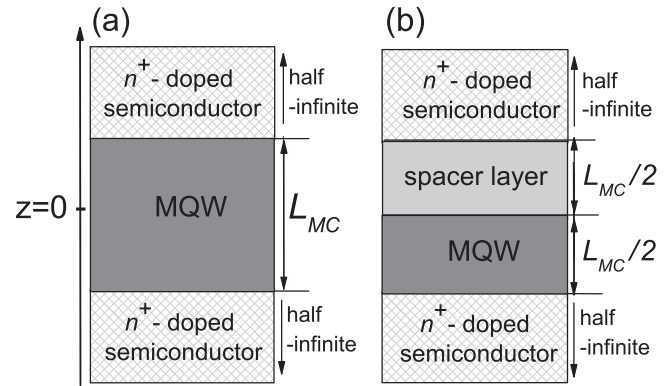

FIG. 1. Diagram illustrating schematically the geometry of the structures discussed in the paper: (a) the three-layer structure and (b) the four-layer structure.

ous that in degenerate structures ($\omega_{\mathrm{IT}} = \omega_{p,\mathrm{mirr}}^{\mathrm{surf}} = \omega_A^{\mathrm{cutoff}}$) the strong (near) resonant coupling of the intersubband excitation with the antisymmetric (for arbitrary $k_\parallel$) and symmetric (but for sufficiently large $k_\parallel$) plasmonic-type modes should be possible.

The above suggestion is consistent with the theoretical study reported in Ref. [39]. The authors of this paper predicted strong coupling interactions between the intersubband excitation and the high-$k_\parallel$ plasmonic-type modes [17] of realistic hyperbolic metamaterials consisting of n^+-doped InGaAs layers and embedded (GaAlAs) MQW slabs. It is also worth noting that a strong coupling between intersubband excitation and the plasmonic-type modes (or more precisely the so-called "epsilon-near-zero" mode [40]) supported by thin n^+-doped semiconductor layer has also been recently reported [41].

This paper provides a detailed theoretical analysis of the properties of the ISPPs branches originated from the S_{SPP} or/and A_{SPP} modes in (nearly degenerate) all-semiconductor plasmonic resonators. We want to stress that in contrast with the earlier papers discussing the resonant coupling between electronic excitation and surface plasmon polariton modes (see, e.g., [18,34]), we do not restrict our discussion to the simplest three-layer geometry, where (cubic) optically active material occupies the whole space between the mirrors. To demonstrate an important role of the symmetry of the resonators in the formation of the multimode ISPP branches (i.e., the branches containing more than one resonator mode [38]), the case of the (asymmetric) four-layer structure shown in Fig. 1(b) is additionally discussed. In this structure, only half of the space between the mirrors is occupied by an active material.

As in our previous papers [37,38], the semiclassical approach based on the transfer matrix formalism and the effective-medium approximation will be employed. The claddings are described by the Drude model. For convenience, calculating the semiclassical dispersion characteristics of the ISPP we neglect, as in Ref. [18], the effects connected with Ohmic losses. Moreover, to get a deeper insight into considered in this work problems we additionally interpret the ISPP characteristics with the help of a simplified quasiparticle (polaritonic) model.

Employing both approaches, we demonstrate, for example, that due to the strong anisotropy of the intersubband excitation, the main conclusions of Ref. [18] are not valid in the case

of the ISPP branches supported by the three-layer structure. We also demonstrate that the dispersion characteristics of the ISPP branches supported by the asymmetric four-layer structures are dramatically affected by the formation of the multimode branches (with a comparable admixture of the two resonator modes). It is worth noting that the similar-type multimode excitonic polaritons have been measured in coupled semiconductor planar MCs [42,43]. Results reported in these papers (see also [44,45]) indicate that physics of multimode polariton branches should be substantially richer than polariton branches occurring due to the single-mode coupling, i.e., the coupling of a single cavity mode with a single electronic excitation.

As mentioned, calculating the dispersion characteristics we neglect losses. It is well known that the omission of the losses does not affect substantially the cavity-polariton characteristics when the coupling mechanism dominates competing loss mechanism. It practically corresponds to the strong coupling regime. We illustrate the usefulness of the lossless characteristics discussed in this paper showing that, to a large extent, they are consistent with the angle-resolved reflection-absorption spectra of the GaAlAs-based realistic structures. We show also that, in the case of the asymmetric structures, the relative height of absorption peaks is strongly sensitive to the location of the MQW slab with respect to the coupling mirror. The effect is qualitatively similar to that observed in coupled semiconductor MCs with a QW located in one of the MCs [42,43,46].

The above findings indicate that it is reasonable to expect that the results reported in this paper will be useful for the analysis of the spectral response and temporal characteristics of the ISPP branches supported by plasmonic resonators. We also suppose that even in the case when spatial damping plays an essential role, the lossless characteristics can be of significance as a fundamental reference.

The paper is organized as follows. Section II presents the description of two types of structures studied in this work. The theoretical framework is given in Secs. III and IV. The characteristics of the electromagnetic modes supported by the passive (i.e., without intersubband excitation) and active structures are presented in Secs. V and VI, respectively. Finally, in Sec. VII we conclude our findings. Appendices A–C contain intermediate analytical results employed in Secs. V and VI. The manifestation of the ISPP branches in the reflection-absorption spectra of the three- and four-layer realistic structures is presented and discussed in Appendix D.

II. DESCRIPTION OF THE STRUCTURES

All-semiconductor resonators considered in this paper are modeled by three- and four-layer (to be more specific, three- and four-media) structures. They are presented in Fig. 1. In both types of structures, the semi-infinite regions $|z| > L_{MC}/2$ are occupied by n^+-doped semiconductor claddings playing the role of mirrors.

In the three-layer (symmetric) structure, the whole space between mirrors is occupied by the MQW slab. In the four-layer (asymmetric) structure, the space between mirrors is occupied by two different layers: the spacer slab and the MQW slab. They have the same thickness ($L_{MC}/2$). The dielectric slab

forming the spacer layer is described by an isotropic relative dielectric constant ε_{spac}.

The MQW slab is modeled by a uniaxial uniform effective medium characterized by the diagonal dielectric tensor with frequency-dependent components $\varepsilon_{MQW,xx} = \varepsilon_{MQW,yy}$ and $\varepsilon_{MQW,zz}$. As mentioned, we omit dissipation. For convenience, we also neglect an intrasubband excitation as well as a small dielectric mismatch between the spacer, the barrier, and well materials. In this limit we get [47]

$$\varepsilon_{MQW,xx} = \varepsilon_w = \varepsilon_{spac}, \tag{1}$$

$$\varepsilon_{MQW,zz} = \varepsilon_w \left(\omega^2 - \omega_{IT}^2\right)/\left(\omega^2 - \omega_{IT}^{*2}\right), \tag{2}$$

where $\omega_{IT}^{*2} = \omega_{IT}^2 - \varpi_{p,MQW}^2$, $\varpi_{p,MQW}^2 = f_{IT}\omega_{p,MQW}^2$, $\omega_{p,MQW}^2 = N_s e^2/d_{MQW} m_w^* \varepsilon_0 \varepsilon_w$, f_{IT} is the oscillator strength connected with the intersubband transition, d_{MQW} (L_{MQW}) is the period (thickness) of the MQW, ε_0 (ε_w) is the vacuum (the well material) dielectric constant, m_w^* is the electron effective mass in the well material, and N_s is the surface electron concentration in the QW. (We work in the two-subband approximation and assume that only the ground subband is occupied.) Moreover, the frequency ω_{IT} corresponds to the frequency of the intersubband Coulomb modes supported by an isolated QW while the frequency ω_{IT}^* coincides with the frequency of the intersubband plasmon propagating along x axes of the infinite MQW [37].

The cladding (mirror) material will be described by a Drude-type dielectric function

$$\varepsilon_{mirr}(\omega) = \varepsilon_c \left(1 - \omega_{p,mirr}^2/\omega^2\right), \tag{3}$$

where $\omega_{p,mirr} = (N_D e^2/m_c^* \varepsilon_0 \varepsilon_c)^{1/2}$ is the plasma frequency of the cladding, ε_c (m_c^*) is the background dielectric constant (electron effective mass) of the claddings, and N_D is the doping density of the cladding material.

In order to minimize the number of relevant parameters, we concentrate on single-material plasmonic resonators where relations $\varepsilon_c = \varepsilon_w$ and $m_c^* = m_w^*$ are approximately valid. In such systems, the ratio $\omega_{p,mirr}^{surf}/\omega_{p,mirr}$ takes the value of $1/\sqrt{2}$. (In the general case, i.e., for $\varepsilon_c \neq \varepsilon_w$ we have $\omega_{p,mirr}^{surf}/\omega_{p,mirr} = 1/\sqrt{1 + \varepsilon_w/\varepsilon_c}$.) Single-material resonators can be grown using molecular beam epitaxy which is a natural technique for growing high-quality plasmonic resonators with embedded QWs [48].

The simplifications described above are approximately fulfilled, for example, in GaAs-based resonators (see, e.g., [10]). In such structures, the expression for $\omega_{p,mirr}$ can be written (taking $\varepsilon_w = 10.9$ and $m_w^* = 0.066\, m_0$, where m_0 is the free-electron mass) as

$$\omega_{p,mirr}(meV) \cong 43.8 \times N_D^{1/2}(10^{18}\, cm^{-3}). \tag{4}$$

For the largest attainable doping level ($N_D = 5.5 \times 10^{18}\, cm^{-3}$) in GaAs [49], we get $\omega_{p,mirr} \cong 102.7$ meV/$\hbar$ and $\omega_{p,mirr}^{surf} \cong 72.62$ meV/$\hbar$ (for single-material resonators). The experimentally obtained value of the plasma frequency, for the above-mentioned value of N_D, is slightly smaller $\omega_{p,mirr} \cong 96.8$ meV/$\hbar$ ($\omega_{p,mirr}^{surf} \cong 68.4$ meV/$\hbar$) [50]. This difference is due to the fact that writing Eq. (4), for simplicity, we have neglected the energy dependence of the (optical) effective

mass in GaAs [51]. A larger value of the mirror plasma frequency can be obtained, for example, replacing GaAs by InGaAs, InAsSb [24,39,41,48,51,52], indium tin oxide (ITO) [33], or ZnO [23]. It is worth also noting that fabrication of n^+InAsSb-GaSb-n^+InAsSb plasmonic resonators, with $\omega_{p,\text{mirr}} \cong 230$ meV/$\hbar$, has recently been reported [53]. Larger than 5×10^{18} cm^{-3} electron concentration in GaAs can be also achieved employing ultrafast optical excitation of photocarriers [54].

III. SEMICLASSICAL APPROACH

A. Transfer matrix formalism

The resonators described in the previous section can be, in general, considered layered structures located between semi-infinite lower (substrate, $j = 0$) and upper (ambient, $j = m + 1$) media with the relative dielectric constant $\varepsilon_{j=0} = \varepsilon_s$ and $\varepsilon_{m+1} = \varepsilon_a$, respectively, where $m = 1,2,3\ldots$ counts the layers of the structures with thickness L_j.

The electric (**E**) and magnetic (**H**) fields of the radiation are taken in the form

$$\mathbf{E}(x,z,t) = [E_x(z),0,E_z(z)]e^{i(k_x x - \omega t)}, \tag{5}$$

$$\mathbf{H}(x,z,t) = [0,H_y(z),0]e^{i(k_x x - \omega t)}, \tag{6}$$

where $k_x(\equiv k_\parallel)$ is the in-plane wave vector. We assume that k_x is a real quantity.

The complex amplitudes of the magnetic field corresponding to the waves traveling in the positive $(+)$ and negative $(-)$ z directions are denoted by $H_{\sigma+}^{(j)}$ and $H_{\sigma-}^{(j)}$, respectively, with $\sigma = l,u$. The subscript l (u) indicates that the amplitude is taken with respect to the plane separating the media j and $j + 1$ $(j - 1$ and j). The relation between amplitudes of the magnetic field in the $j = 0$ (substrate) and $j = m + 1$ (ambient) media may be written as [47]

$$\begin{bmatrix} H_{l+}^{(0)} \\ H_{l-}^{(0)} \end{bmatrix} = \mathbf{T} \begin{bmatrix} H_{u+}^{(m+1)} \\ H_{u-}^{(m+1)} \end{bmatrix}, \tag{7}$$

where $\mathbf{T} = \mathbf{I}_{0,1}\mathbf{L}_1\mathbf{I}_{1,2}\ldots\mathbf{L}_m\mathbf{I}_{m,m+1}$ is the transfer matrix of the structure. Matrix $\mathbf{I}_{\kappa,j} \equiv \mathbf{I}(r_{\kappa,j})$, accounting for the interface between the media (layers) κ and $j(=\kappa + 1)$, is given by

$$\mathbf{I}(r_{\kappa,j}) = \mathbf{I}^{-1}(r_{j,\kappa}) \equiv \frac{1}{t_{\kappa,j}} \begin{bmatrix} 1 & r_{\kappa,j} \\ r_{\kappa,j} & 1 \end{bmatrix}, \tag{8}$$

where $r_{j,\kappa}$ $(t_{\kappa,j})$ is the Fresnel reflection (transmission) coefficient.

Matrix $\mathbf{L}_j$, describing the propagation through the jth layer, is given by

$$\mathbf{L}_j = \begin{bmatrix} e^{-ik_{j,z}L_j} & 0 \\ 0 & e^{ik_{j,z}L_j} \end{bmatrix}, \tag{9}$$

where $k_{j,z}$ is the normal component of the wave vector in the jth medium. In the approximation used here we get [10,37,47]

$$k_{\nu,z} = \begin{cases} \sqrt{\varepsilon_w(K^2 - k_x^2/\varepsilon_{\text{MQW},z})}, & \nu = \text{MQW} \\ \sqrt{\varepsilon_{\text{mirr}}K^2 - k_x^2}, & \nu = \text{mirr} \\ \sqrt{\varepsilon_w K^2 - k_x^2}, & \nu = \text{spac} \end{cases} \tag{10}$$

where $K = \omega/c$ and c is the speed of light in the vacuum. In further discussion the quantity $k_{\nu,z}$, defined by Eq. (10), will be represented as $i\alpha_\nu$.

B. Characteristic equations

The characteristic equation for electromagnetic modes supported by the multilayer structure can be obtained from the requirement that no light incidents on the MC from outside. Employing this requirement, we get $T_{11} = 0$ [37,38]. It implies the following eigenequation for the four-layer structure [55]

$$\left[1 + \tanh\left(\alpha_{\text{spac}} \frac{L_{\text{MC}}}{2}\right) \frac{\alpha_{\text{spac}}\varepsilon_{\text{mirr}}}{\varepsilon_{\text{spac}}\alpha_{\text{mirr}}} \right]$$
$$\times \left[1 + \tanh\left(\alpha_{\text{MQW}} \frac{L_{\text{MC}}}{2}\right) \frac{\alpha_{\text{mirr}}\varepsilon_{\text{spac}}}{\varepsilon_{\text{mirr}}\alpha_{\text{MQW}}} \right]$$
$$+ \left[1 + \tanh\left(\alpha_{\text{spac}} \frac{L_{\text{MC}}}{2}\right) \frac{\alpha_{\text{mirr}}\varepsilon_{\text{spac}}}{\varepsilon_{\text{mirr}}\alpha_{\text{spac}}} \right]$$
$$\times \left[1 + \tanh\left(\alpha_{\text{MQW}} \frac{L_{\text{MC}}}{2}\right) \frac{\varepsilon_{\text{mirr}}\alpha_{\text{MQW}}}{\alpha_{\text{mirr}}\varepsilon_{\text{spac}}} \right] = 0. \tag{11}$$

When we replace the spacer layer by the MQW slab, then the above equation transforms into the eigenequation for the three-layer structure:

$$\tanh\left(\alpha_{\text{MQW}} \frac{L_{\text{MC}}}{2}\right) = -\left(\frac{\alpha_{\text{mirr}}\varepsilon_{\text{spac}}}{\varepsilon_{\text{mirr}}\alpha_{\text{MQW}}}\right)^{\pm 1}. \tag{12}$$

The $\pm$ signs, in Eq. (12), correspond to the symmetric and antisymmetric modes, respectively. [The symmetry is defined with respect to the z component of the electric field $E_z(z)$.]

Let us assume that, like in the structure discussed in Appendix D, the transmission through one of the mirrors (the coupling mirror) can be taken as nonzero. Then, the absorptance (equal to the fraction of the incident energy absorbed) of the structure is given by $A = 1 - |r|^2$ where $r = T_{21}/T_{11}$ is the complex reflection coefficient of the structure [37,47].

To make our results as general as possible, we introduce, following [10,17], dimensionless (normalized) quantities

$$\bar{z} = zk_\perp, \quad \bar{k}_x = k_x/k_\perp, \quad \bar{\alpha}_\nu = \alpha_\nu/k_\perp, \quad \bar{\omega} = \omega/\omega_\perp,$$
$$\bar{\omega}_{\text{IT}} = \omega_{\text{IT}}/\omega_\perp, \quad \bar{\omega}_{p,\text{mirr/MQW}} = \omega_{p,\text{mirr/MQW}}/\omega_\perp, \tag{13}$$

where $k_\perp = \pi/L_{\text{MC}}$ and $\omega_\perp = \pi c/L_{\text{MC}}\sqrt{\varepsilon_w}$. The normalization frequency $\omega_\perp$, appearing in Eq. (13), coincides with the cutoff frequency of the TM$_1$ mode supported by the MC with perfect mirrors [see Eq. (B15)].

One finds that in the case of a single-material resonator, the following useful relations are valid:

$$\bar{\alpha}_{\text{spac}}^2 = \bar{k}_x^2 - \bar{\omega}^2, \tag{14}$$

$$\bar{\alpha}_{\text{mirr}}^2 = \bar{\alpha}_{\text{spac}}^2 + \bar{\omega}_{p,\text{mirr}}^2, \tag{15}$$

$$\bar{\alpha}_{\text{MQW}}^2 = \bar{\alpha}_{\text{spac}}^2 + \bar{k}_x^2\bar{\omega}_{p,\text{MQW}}^2/(\bar{\omega}^2 - \bar{\omega}_{\text{IT}}^2), \tag{16}$$

$$\varepsilon_{\text{mirr}} = \varepsilon_w(1 - \bar{\omega}_{p,\text{mirr}}^2/\bar{\omega}^2). \tag{17}$$

Moreover, in the case of GaAs-based resonators we get

$$\omega_\perp(\text{meV}) \cong 187.8 \times L_{\text{MC}}^{-1} \, (\mu\text{m}), \tag{18}$$

$$\bar{\omega}_{p,\text{mirr}} \cong 0.23 \times N_D^{1/2}(10^{18} \, \text{cm}^{-3})L_{\text{MC}} \, (\mu\text{m}). \tag{19}$$

IV. ANALYTIC MODEL

In addition to the numerical study, based on the dispersion equations (11) and (12), we will give a simplified analytical description of the ISPP branches. It is based on the quasiparticle picture and employs the concept of the generalized mode overlap factor. The single and multimode couplings will be discussed. The latter case corresponds to the situation where two or more resonator modes are simultaneously involved in the formation of the ISPP branches [38].

A. Strong coupling between cavity mode and intersubband excitation: Microscopic approach

It is well known that a rigorous description of strong coupling requires a quantum-mechanical model not only for the intersubband excitation, but also for the resonator modes. Such a fully quantum-mechanical approach has been used in Ref. [5] (see also [56]) for the discussion of the intersubband cavity polariton supported by semiconductor MCs. Results reported in Ref. [5] indicate that, due to the collective nature of the intersubband excitation, the dipole representation of the Coulomb gauge is particularly suitable to describe such an excitation. One of its advantages is that the interwell coupling is mediated entirely by the cavity photons.

In what follows, we employ the fact that when we work in the above-mentioned gauge, the coupling strength of the collective intersubband excitation and the nth photonic mode supported by the semiconductor MC can be treated as proportional to the spatial overlap integral $\int_{\text{MQW}}(\varepsilon_0\varepsilon_w)^{-1}D_{n,z}P_{\text{MQW},z}dz$ [5,57]. Here, $\mathbf{P}_{\text{MQW}}$ is the microscopical average intersubband polarization density of the MQW slab and $\mathbf{D}_n$ the displacement field corresponding to the nth photonic mode. Since the intersubband transitions are associated with a dipole oscillation along the growth direction z, only the components $D_{n,z}$ and $P_{\text{MQW},z}$ appear in the overlap integral.

The phenomenon of the vacuum Rabi splitting comes from interaction of the vacuum field of the resonator with electronic excitation. It means that calculating the above-mentioned overlap integral we should correctly normalize the function $D_{n,z}$. Namely, the total electromagnetic field energy (per unit area) of the nth mode (U_n^{total}) should coincide with $\hbar\omega_n/2$. In other words, $|D_{n,z}|^2$ should be divided by the normalization factor α_n given by [5,58]

$$
\begin{aligned}
\alpha_n &= \frac{1}{\hbar\omega_n}\int_{-\infty}^{\infty}dz\{[\varepsilon_0\varepsilon(z)]^{-1}|\mathbf{D}_n(z)|^2 + \mu_0|\mathbf{H}_n(z)|^2\} \\
&= \frac{2}{\hbar\omega_n}\int_{-\infty}^{\infty}dz\{[\varepsilon_0\varepsilon(z)]^{-1}|\mathbf{D}_n(z)|^2\},
\end{aligned} \tag{20}
$$

where $\mathbf{H}_n$ is the magnetic field of the nth mode, μ_0 is the magnetic constant of the vacuum, and $\varepsilon(z)$ is the spatial-dependent dielectric function of the resonator. (Note that having $D_{n,z}$ we can calculate $D_{n,x}$ and $H_{n,y}$ employing relations given in Appendix B.)

Below, we generalize the above normalization procedure on the case of the plasmonic-type modes. In Sec. IV we present numerical results showing that, obtained in this way, ISPP characteristics are consistent with the characteristics predicted by the semiclassical approach described in Sec. III.

B. Single-mode coupling: Basic concepts

In this section we focus on the three-layer (symmetric) structures assuming that the physics devoted to the formation of the ISPP branches is well captured by the single-mode cavity approximation. It means that each resonator mode originates only two (upper and lower) ISPP branches. Below, we derive secular equation describing the properties of the above-mentioned branches.

1. Bright and dark intersubband excitations

Discussing the strong coupling between the cavity modes and intersubband excitations supported by the QWs embedded into the resonator, it is convenient to introduce a useful concept of the bright and dark intersubband excitations. A simplified formulation of this concept has been discussed in our previous paper [38] (see also [59]). Such a formulation is sufficient for our purpose. (Rigorous justification of the approach developed in Ref. [38] can be found in Refs. [56,60].)

Let us denote the intersubband (polarization) state of the ιth QW (located at $z = z_\iota$, $\iota = 1,2,3\ldots N_{\text{QW}}$) by $\mathcal{P}_\iota^{\text{QW}}$. For convenience, the in-plane wave vector $\bar{k}_x$ will be omitted. We focus on the description of the coupling between the above-mentioned QWs and the resonant cavity mode (n_{res}) having the frequency $\omega_{n_{\text{res}}} \approx \omega_{\text{IT}}$. This description simplifies greatly when we introduce, like in Ref. [38], the following new bases for the intersubband states supported by the whole MQW slab:

$$
P_{\mu,n_{\text{res}}}^{\text{MQW}} = \sum_{\iota=1}^{N_{\text{QW}}} C_\iota^{(\mu,n_{\text{res}})}\mathcal{P}_\iota^{\text{QW}}. \tag{21}
$$

The quantities $P_{\mu,n_{\text{res}}}^{\text{MQW}}$'s ($\mu = 1,2,3\ldots N_{\text{QW}}$) represent the intersubband excitations delocalized over the N_{QW} quantum wells according to the specific coherent linear combinations of the original single-well states $\mathcal{P}_\iota^{\text{QW}}$.

For the so-called bright excitation ($\mu = 1$), associated with the resonant mode, we take

$$
C_\iota^{(1,n_{\text{res}})} = f_{n_{\text{res}},z}(z_\iota)\bigg/\sqrt{\sum_{\iota=1}^{N_{\text{QW}}}|f_{n_{\text{res}},z}(z_\iota)|^2}, \tag{22}
$$

where the (dimensionless) mode function $f_{n_{\text{res}},z}(z)$ describes the spatial variation of $D_{n_{\text{res}},z}$ (see Appendix B).

The remaining $N_{\text{QW}} - 1$ dark states $P_{\mu',n_{\text{res}}}^{\text{MQW}}$ ($\mu' = 2,3,4\ldots N_{\text{QW}}$) are characterized by the N_{QW} component vectors $\mathbf{C}^{(\mu',n_{\text{res}})}$ which are orthogonal to the vector $\mathbf{C}^{(1,n_{\text{res}})}$. It means that the dark excitations ($P_{\mu',n_{\text{res}}}^{\text{MQW}}$) do not couple to the mode n_{res} [38,56].

The above discussion suggests that (when we work in the single-mode cavity approximation) it is very convenient to model the electronic system by the (effective/collective) excitations corresponding, not to the individual QWs, but to the (degenerate and delocalized over the whole MQW) the bright ($P_{1,n_{\text{res}}}^{\text{MQW}}$) and dark ($P_{\mu',n_{\text{res}}}^{\text{MQW}}$) intersubband excitations.

In further discussion, we employ the fact that the semiclassical approach discussed in Sec. III, as well as the quantum-mechanical approach developed in Ref. [5], is based on the long-wavelength approximation. In other words, we can assume that D_z, associated with electromagnetic field interacting with intersubband excitations, varies slowly on the period of

the MQW slab (d_{MQW}). Consequently, the spatial averaging (over the MQW period) of the localized intersubband polarization supported by the wells is justified (for details, see [47]). Employing this simplification one finds that, in the case of the structures with large number of the wells ($N_{\mathrm{QW}} \gg 1$), the spatial variation of the (averaged) intersubband polarization, associated with the bright excitation $P_{1,n_{\mathrm{res}}}$, can be described by the mode function $f_{n_{\mathrm{res}},z}$.

2. "Diagonal" coupling and in-gap polariton branches

Let us assume for simplicity that the MQW slab (with $N_{\mathrm{QW}} \gg 1$) occupies the whole space between a nearly perfect metallic mirror and that the ground cavity mode is resonant with intersubband transitions ($n_{\mathrm{res}} = \mathrm{TEM}$). Then, the (averaged) spatial variation of the bright excitation $P_{1,\mathrm{TEM}}^{\mathrm{MQW}}$ coincides with the spatial variation of the ground resonator mode. Since mirrors are perfect, cavity modes vanish outside the region occupied by the MQW (i.e., in the mirrors). It implies that the (averaged) spatial variations of the dark excitations $P_{\mu'=2,3\ldots N_{\mathrm{QW}},\mathrm{TEM}}^{\mathrm{MQW}}$ coincide with the spatial variations of appropriate higher cavity modes $\mathrm{TM}_{\mu'=2,3\ldots N_{\mathrm{QW}}}$. Thus (restricting for simplicity to the RWA), one finds that the system Hamiltonian, written in the basis $P_{\mu,\mathrm{TEM}}^{\mathrm{MQW}}$, will have a block-diagonal form. Equivalently, we can say that a separate 2×2 Hamiltonian [leading to the secular equation having the same form as Eq. (34)] is only needed for each (ground or excited) cavity mode. It means that, in addition to the resonant coupling between the transverse electromagnetic (TEM) mode and the bright excitation $P_{1,\mathrm{TEM}}^{\mathrm{MQW}}$, also the nonresonant coupling of the dark intersubband excitations $P_{\mu',\mathrm{TEM}}^{\mathrm{MQW}}$ with higher photonic modes $\mathrm{TM}_{\mu'}$ has to be considered. Since the above-mentioned couplings take place between the photonic modes and the intersubband excitations having the same spatial variation, it is reasonable to speak about the nonresonant "diagonal" coupling [38]. The presence of such coupling can be associated with the formation of weakly dispersive (higher-order) intersubband polariton branches. They are located slightly below ω_{IT}, i.e., in the polariton gap region. In the literature, these branches are named as the in-gap polaritons [61]. They contain a very small admixture of higher photonic modes [38,61]. (We assume that the coupling frequency with higher modes is much smaller than the cavity-mode separation.)

It is obvious that the penetration of the cavity mode into the mirrors leads to the violation of the single-mode cavity approximation. Fortunately, in the case of typical symmetric structures, consequences resulting from the violation of the single-mode coupling can be neglected in the first approximation (see Sec. IV C 1).

3. Secular equation and the generalized mode overlap factor

a. Nondispersive mirrors. The description of the vacuum Rabi splitting simplifies dramatically when intersubband excitation couples resonantly only with the TEM mode (i.e., $n_{\mathrm{res}} = \mathrm{TEM}$). It is connected with the fact that $D_{\mathrm{TEM}} = |D_{\mathrm{TEM},z}| = $ const in the region occupied by the MQW and $D_{\mathrm{TEM}} = 0$ outside this region, i.e., inside the mirrors. Then, we can speak about the perfect overlap of the (averaged) intersubband

polarization associated with the bright excitation $P_{1,\mathrm{TEM}}^{\mathrm{MQW}}$ and the TEM mode field.

The fully quantum-mechanical approach or semiclassical approach leads to the following secular equation for the intersubband polariton branches originating from the TEM mode in the three-layer structure [5,37]:

$$\left(\bar{\omega}^2 - \bar{\omega}_{\mathrm{TEM}}^2\right)\left(\bar{\omega}^2 - \bar{\omega}_{\mathrm{IT}}^2\right) = 4\bar{\omega}_{\mathrm{TEM}}^2 \bar{\Omega}_{R,\mathrm{TEM}}^2, \qquad (23)$$

where $\bar{\omega}_{\mathrm{TEM}} = \bar{k}_x$ is the (normalized) frequency of the TEM mode [see Eq. (B15)]. For the (normalized) coupling frequency $\bar{\Omega}_{R,\mathrm{TEM}} = \Omega_{R,\mathrm{TEM}}/\omega_\perp$ we get the expression $\bar{\Omega}_{R,\mathrm{TEM}} = \bar{\varpi}_{p,\mathrm{MQW}}/2$ where $\bar{\varpi}_{p,\mathrm{MQW}}$ is defined in Sec. II. [We would like to stress that Eq. (23) is not based on the random wave approximation (RWA).]

In the case of the structures with realistic mirrors, the above-mentioned overlap is not perfect. It is associated mainly with the penetration of the cavity mode into the region occupied by the mirrors. Moreover, we should also remember that the relation $D_n = |D_{n,z}|$ is not valid even in the case of the ground mode. The consequences of these facts can be included employing the concept of the mode overlap factor. The formula for this factor was first reported heuristically in Refs. [56,59] (see also [62]).

Taking into account the normalization procedure of the cavity field described above [(see Eq. (20)] as well as employing the concept of the bright intersubband excitation corresponding to the resonant photonic mode one finds that the secular equation (23) for the TEM mode can be extended in the case of the structure with nonperfect dielectric mirrors in the following way. Namely, $\bar{\omega}_{\mathrm{TEM}}$ should be replaced by $\bar{\omega}_{n_{\mathrm{res}}}$ (= the normalized frequency of the resonant cavity mode). Moreover, $\bar{\Omega}_{R,\mathrm{TEM}}$ should be replaced by the (normalized) coupling frequency $\bar{\Omega}_{R,n_{\mathrm{res}}}$, corresponding to the resonant mode. This frequency can be written as a product $\bar{\Omega}_{R,n_{\mathrm{res}}} = \bar{\Omega}_{R,\mathrm{TEM}} F_{n_{\mathrm{res}},z}^{1/2}$ where the mode overlap factor $F_{n,z}$ is defined by [5,56,59,62]

$$F_{n,z} \equiv \frac{U_{n,z}^{\mathrm{spac}}}{U_n^{\mathrm{total}}} = \frac{\int_{\mathrm{spac}} \varepsilon_w^{-1} |D_{n,z}(z)|^2 dz}{\int_{-\infty}^{\infty} \varepsilon^{-1}(z) |\mathbf{D}_n(z)|^2 dz}. \qquad (24)$$

Here, $U_{n,z}^{\mathrm{spac}}$ is the electromagnetic energy contained in the z component of the displacement $\mathbf{D}_n$ in the spacer layer, i.e., in the region occupied by the MQW.

We would like to stress that the factor $F_{n,z}$ describes the reduction of the coupling frequency resulting from the penetration of the cavity mode into the mirrors as well as takes into account the anisotropy of the intersubband excitation. It is manifested by the fact that, compared to the normalization factor α_n [see Eq. (20)], the quantity $F_{n,z}$ is additionally controlled by the spatial variation of $D_{n,z}$ in the region occupied by the MQW slab. Thus, the quantity $F_{n,z}$ can be called the "projected" nth-mode overlap factor. In the idealized case of perfect dielectric mirrors, Eq. (24) simplifies to the form

$$F_{n,z}^{\mathrm{perf}} = \bar{k}_x^2 / \left(\bar{k}_x^2 + n^2\right). \qquad (25)$$

b. Dispersive mirrors. Now we assume, motivated by the papers [57,58,60,63–65], that the concept of the mode overlap factor developed for the photonic-type modes can be adapted for the plasmonic-type modes. It means that the generalized

secular equation, corresponding to the $\mathcal{N}$th plasmonic mode, can be taken in the following form:

$$\left(\bar{\omega}^2 - \bar{\omega}_{\mathcal{N}}^2\right)\left(\bar{\omega}^2 - \bar{\omega}_{\mathrm{IT}}^2\right) = 4\bar{\omega}_{\mathcal{N}}^2\bar{\Omega}_{R,\mathcal{N}}^2, \tag{26}$$

where $\bar{\omega}_{\mathcal{N}}$ is the normalized frequency of the $\mathcal{N}$th plasmonic mode. The coupling frequency $\bar{\Omega}_{R,\mathcal{N}}$ (corresponding to the $\mathcal{N}$th mode) can also be written as a product

$$\bar{\Omega}_{R,\mathcal{N}} = \bar{\Omega}_{R,\mathrm{TEM}}F_{\mathcal{N},z}^{1/2}. \tag{27}$$

The overlap factor appearing in this equation is defined as $F_{\mathcal{N},z} = U_{\mathcal{N},z}^{\mathrm{spac}}/U_{\mathcal{N}}^{\mathrm{total}}$ where $U_{\mathcal{N},z}^{\mathrm{spac}}$ is the electromagnetic energy contained in the z component of $\mathbf{D}_{\mathcal{N}}$ in the spacer-layer region. $U_{\mathcal{N}}^{\mathrm{total}}$ is the total electromagnetic energy.

Although the formal expression for the mode overlap factor is the same as for structures with dispersive and nondispersive mirrors, it is essential to include the fact that Eq. (20) is not valid for dispersive media. Following [12,63,66,67], the expression for the energy density associated with the $\mathcal{N}$th mode is taken in the form

$$\mathcal{U}_{\mathcal{N}}(z) = \frac{1}{2}\left\{ \frac{1}{\varepsilon_0 \varepsilon^2(z,\omega_{\mathcal{N}})} \frac{\partial[\omega'\varepsilon(z,\omega')]}{\partial\omega'}\bigg|_{\omega'=\omega_{\mathcal{N}}} |\mathbf{D}_{\mathcal{N}}(z)|^2 \right.$$
$$\left. + \mu_0|\mathbf{H}_{\mathcal{N}}(z)|^2 \right\}, \tag{28}$$

where $\mathbf{H}_{\mathcal{N}}$ is the magnetic field of the $\mathcal{N}$th plasmonic mode. The spatial-dependent dielectric function $\varepsilon(z,\omega)$ characterizing the structure is defined by Eq. (B4).

Calculating the total energy $U_{\mathcal{N}}^{\mathrm{total}} = \int_{-\infty}^{\infty} \mathcal{U}_{\mathcal{N}}(z)dz$ we can eliminate $|\mathbf{H}_{\mathcal{N}}(z)|^2$ appearing in Eq. (28) employing the identity derived by Chang and Chuang [see Eq. (11) in Ref. [64]]. Performing appropriate manipulations we get

$$U_{\mathcal{N}}^{\mathrm{total}} = \int_{-\infty}^{\infty} \frac{1}{\varepsilon_0 \varepsilon_g(z,\omega_{\mathcal{N}})} |\mathbf{D}_{\mathcal{N}}|^2 dz, \tag{29}$$

where

$$\frac{1}{\varepsilon_g(z,\omega_{\mathcal{N}})} = \frac{1}{\varepsilon(z,\omega_{\mathcal{N}})} - \frac{\omega_{\mathcal{N}}}{2}\frac{\partial}{\partial\omega'}\frac{1}{\varepsilon(z,\omega')}\bigg|_{\omega'=\omega_{\mathcal{N}}}. \tag{30}$$

Substituting Eqs. (B4) and (3) into Eq. (30) we obtain

$$\varepsilon_g(z,\omega_{\mathcal{N}}) = \begin{cases} \varepsilon_w & \text{for } |z| < L_{\mathrm{MC}}/2, \\ \varepsilon_{\mathrm{mirr}}^2(\omega_{\mathcal{N}})/\varepsilon_w & \text{for } |z| > L_{\mathrm{MC}}/2. \end{cases} \tag{31}$$

If we take into account (31) and employ the fact that due to the symmetry of the structure $|\mathbf{D}_{\mathcal{N}}(z)| = |\mathbf{D}_{\mathcal{N}}(-z)|$, the expression for the total energy (29) simplifies to

$$U_{\mathcal{N}}^{\mathrm{total}} = \frac{2}{\varepsilon_0}\left[\frac{1}{\varepsilon_w}\int_0^{L_{\mathrm{MC}}/2} |\mathbf{D}_{\mathcal{N}}|^2 dz + \frac{\varepsilon_w}{\varepsilon_{\mathrm{mirr}}^2(\omega_{\mathcal{N}})}\int_{L_{\mathrm{MC}}/2}^{\infty} |\mathbf{D}_{\mathcal{N}}|^2 dz \right]$$
$$= 2\int_0^{\infty} \varepsilon_0 \varepsilon_w |\mathbf{E}_{\mathcal{N}}|^2 dz. \tag{32}$$

It is worth noting that the described above normalization procedure is consistent with the results reported in Ref. [68] (see also [69–71]) where a Hamiltonian formulation of electromagnetic fields in dispersive structured media has been used.

Employing Eqs. (29)–(32), we find that the expression for the generalized mode overlap factor $F_{\mathcal{N},z} = U_{\mathcal{N},z}^{\mathrm{spac}}/U_{\mathcal{N}}^{\mathrm{total}}$ can

be rewritten as

$$F_{\mathcal{N},z} = \int_0^{L_{\mathrm{MC}}/2} |E_{\mathcal{N},z}|^2 dz / \int_0^{\infty} |\mathbf{E}_{\mathcal{N}}|^2 dz. \tag{33}$$

c. The two-coupled-oscillator model. When the dimensionless coupling factor $g_{\mathcal{N}} = \bar{\Omega}_{R,\mathcal{N}}/\bar{\omega}_{\mathrm{IT}}$ is small ($\lesssim 0.1$) and simultaneously $\bar{k}_x$ is close to its resonant value $\bar{k}_{\mathcal{N}}^{\mathrm{res}}$ (at which $\bar{\omega}_{\mathcal{N}} = \bar{\omega}_{\mathrm{IT}}$), Eq. (26) is well approximated by a secular equation

$$(\bar{\omega} - \bar{\omega}_{\mathcal{N}})(\bar{\omega} - \bar{\omega}_{\mathrm{IT}}) = \left(\bar{\Omega}_{R,\mathcal{N}}^{\mathrm{res}}\right)^2, \tag{34}$$

predicted by the commonly used two-coupled-oscillator model (based on the RWA). Note that in this approximation we neglect $\bar{k}_x$ dependence of the coupling frequency, i.e., we replace $\bar{\Omega}_{R,\mathcal{N}}$ by $\bar{\Omega}_{R,\mathcal{N}}^{\mathrm{res}} = \bar{\Omega}_{R,\mathcal{N}}(\bar{k}_{\mathcal{N}} = \bar{k}_{\mathcal{N}}^{\mathrm{res}})$. Both equations (26) and (34) predict the anticrossing behavior of the ISPP branches when $\bar{\omega}_{\mathcal{N}}$ is close to $\bar{\omega}_{\mathrm{IT}}$. However, it is worth stressing that the polariton branches resulting from Eq. (26) are slightly red-shifted with respect to the results predicted by a simplified Eq. (34). For example, employing Eq. (26) one finds that at $\bar{k}_x = \bar{k}_{\mathcal{N}}^{\mathrm{res}}$, the (normalized) frequency of the upper ($\mathcal{N}_{\mathrm{ISPP}}^U$) and lower ($\mathcal{N}_{\mathrm{ISPP}}^L$) ISPP branches can be written as $\bar{\omega}_{\mathcal{N}_{\mathrm{ISPP}}^{U/L}}^{\mathrm{res}} = \bar{\omega}_{\mathrm{IT}}(1 \pm 2g_{\mathcal{N}}^{\mathrm{res}})^{1/2}$ where $g_{\mathcal{N}}^{\mathrm{res}} = g_{\mathcal{N}}(\bar{k}_x = \bar{k}_{\mathcal{N}}^{\mathrm{res}})$. On the other hand, using Eq. (34) we get $\bar{\omega}_{\mathcal{N}_{\mathrm{ISPP}}^{U/L}}^{\mathrm{res}} = \bar{\omega}_{\mathrm{IT}}(1 \pm g_{\mathcal{N}}^{\mathrm{res}})$. It means that only in the limit $g_{\mathcal{N}} \lesssim 0.1$ the frequencies $\bar{\omega}_{\mathcal{N}_{\mathrm{ISPP}}^{U/L}}^{\mathrm{res}}$ are nearly symmetrically positioned with respect to $\bar{\omega}_{\mathrm{IT}}$. The resonant branch separation $\bar{\Delta}_{\mathcal{N}_{\mathrm{ISPP}}}^{\mathrm{res}} = \bar{\omega}_{\mathcal{N}_{\mathrm{ISPP}}^U}^{\mathrm{res}} - \bar{\omega}_{\mathcal{N}_{\mathrm{ISPP}}^L}^{\mathrm{res}}$ coincides then with the double value of the resonant coupling frequency $\bar{\Delta}_{\mathcal{N}_{\mathrm{ISPP}}}^{\mathrm{res}} = 2\bar{\Omega}_{R,\mathcal{N}}^{\mathrm{res}}$. Moreover, Eq. (26), in contrast with simplified Eq. (34), predicts the formation of the polariton gap. For illustration, when $\omega_{\mathrm{IT}}^2 \ll (\omega_{p,\mathrm{mirr}}^{\mathrm{surf}})^2$ we get a well-known result. Namely, in the case of the ISPP branches originating from the S_{SPP} mode, the polariton gap is positioned between ω_{IT}^* and ω_{IT} [5,37] (see also Fig. 9).

As mentioned, writing Eq. (33) for the generalized mode overlap factor we have considered the (symmetric) three-layer structures. It is obvious that in the case of the (asymmetric) four-layer structures, i.e., when only half of the space between the mirrors is occupied by the MQW, the corresponding overlap factor $F_{\mathcal{N},z} (\equiv F_{\mathcal{N},z}^{\mathrm{asymm}})$ is smaller than one obtained for the symmetric structure $F_{\mathcal{N},z} (\equiv F_{\mathcal{N},z}^{\mathrm{symm}})$. Employing the equality $|\mathbf{E}_{\mathcal{N}}(z)| = |\mathbf{E}_{\mathcal{N}}(-z)|$, we find that $F_{\mathcal{N},z}^{\mathrm{asymm}} = F_{\mathcal{N},z}^{\mathrm{symm}}/2$.

A more general case, when QWs are arbitrarily located between the mirrors couple with the $\mathcal{N}$th mode, is briefly discussed in Appendix A.

C. Multimode coupling in four-layer structures

So far we have assumed that the physics devoted to the formation of the ISPP branches is well described by the single-mode cavity approximation. It has a very good justification in the case of the three-layer systems with perfect mirrors. In general, this approximation works well also in the realistic systems provided that the coupling frequency is substantially smaller than the separation between cavity modes. We know, however, that in plasmonic resonators, the separation between the plasmonic modes decreases with increasing $\bar{k}_x$. Consequently, the condition when the resonant coupling frequency is comparable with the plasmonic mode separation can be relatively easily achieved at $\bar{k}_x \gtrsim 1$. It means

that in the case of the asymmetric plasmonic resonators, the formation of (hybrid) multimode ISPP branches containing simultaneous admixture of the S_{SPP} and A_{SPP} modes should be also considered. In other words, we should go beyond the single-mode approximation or more precisely beyond "diagonal" coupling. Below, we present (employing the RWA) a simplified description of the formation of such hybrid-type branches in the degenerate four-layer structures.

1. "Nondiagonal" coupling

Let us assume that the spatial extent of the cavity modes substantially exceeds the MQW thickness (L_{MQW}). It takes place when L_{MQW} is substantially smaller than L_{MC} or/and when the cavity modes penetrate strongly into the mirrors. In such system the bright intersubband excitation $P_{1,n_{\text{res}}}^{\text{MQW}}$ associated with the resonant mode may not be treated as orthogonal to the nonresonant cavity modes ($n \neq n_{\text{res}}$). Then, it is convenient to introduce, in addition to the above discussed "diagonal" coupling, the concept of the "nondiagonal" coupling corresponding to the coupling between the bright intersubband excitation $P_{1,n_{\text{res}}}^{\text{MQW}}$ and the nonresonant ($n \neq n_{\text{res}}$) cavity modes [38].

It is obvious that in the case of the three-layer plasmonic structures the simultaneous coupling of the two plasmonic modes to the same bright intersubband excitation (e.g., $P_{1,A}^{\text{MQW}}$) is forbidden by the symmetry. It (practically) means that in the symmetric structures the nondiagonal coupling is strongly nonresonant. Consequently, its influence on the dispersion characteristics of the ISPP branches supported by symmetric systems can be neglected in the first approximation. In the case of the asymmetric structures, the nondiagonal coupling is not forbidden. Thus, it is reasonable to expect that in asymmetric plasmonic resonators the formation of hybrid multimode ISPP branches should play an important role.

2. Multimode polaritons in degenerate four-layer structures: Three-coupled-oscillator model

To get useful analytical results, we focus on the degenerate ($\bar{\omega}_{\text{IT}} = \bar{\omega}_{p,\text{mirr}} = \bar{\omega}_A^{\text{cutoff}}$) four-layer structures. In such structures, two plasmonic modes, one with the strong dispersion (i.e., the S_{SPP} mode) and the other one quasidispersionless (i.e., the A_{SPP} mode), can simultaneously interact with the same intersubband excitation (e.g., the bright excitation $P_{1,A}^{\text{MQW}}$). At this point, it is worth noting that a very similar situation has recently been studied theoretically and experimentally by Zhang *et al.* [72]. The authors demonstrate the hybrid coupling among molecular excitons, surface plasmon polariton, and Fabry-Perot mode in a nanostructured metallic cavity. (Mentioned in the Introduction, paper [45], in contrast with [42–44,72] and this paper, discusses the strong coupling between a single-cavity mode and many nondegenerate electronic excitations.)

Now, we show that, within the RWA, the main polaritonic properties of the degenerate four-layer structures are (as in the systems studied in Ref. [72]) reasonably well captured by the three-coupled-oscillator model.

The coupling of the nearly resonant mode A_{SPP} with the bright intersubband excitation $P_{1,A}^{\text{MQW}}$ is quantified by the $\bar{k}_x$-dependent frequency $\bar{\Omega}_{R,A}$. This coupling leads to the

formation of the branches A_{ISPP}^U and A_{ISPP}^L which are a linear combination of the A_{SPP} mode and the $P_{1,A}^{\text{MQW}}$ excitation. They can be modeled by two effective oscillators. The frequencies of these oscillators are given by the (simplified) secular equation (34). Since the structure here considered is asymmetric, the nondiagonal coupling of the S_{SPP} mode with the bright intersubband excitation $P_{1,A}^{\text{MQW}}$ is possible. It means that both effective oscillators, modeling branches A_{ISPP}^U and A_{ISPP}^L, couple with the oscillator modeling the S_{SPP} mode. Such a hybrid coupling is approximately described by a three-coupled-oscillator model expressed as

$$\begin{vmatrix} \bar{\omega}_S - \bar{\omega} & \bar{\Omega}_{S,A_{\text{ISPP}}^U} & \bar{\Omega}_{S,A_{\text{ISPP}}^L} \\ \bar{\Omega}_{S,A_{\text{ISPP}}^U} & \bar{\omega}_{A_{\text{ISPP}}^U} - \bar{\omega} & 0 \\ \bar{\Omega}_{S,A_{\text{ISPP}}^L} & 0 & \bar{\omega}_{A_{\text{ISPP}}^L} - \bar{\omega} \end{vmatrix} = 0, \qquad (35)$$

where $\bar{\Omega}_{S,A_{\text{ISPP}}^U}$ ($\bar{\Omega}_{S,A_{\text{ISPP}}^L}$) is the normalized coupling frequency between the S_{SPP} mode and the A_{ISPP}^U (A_{ISPP}^L) branch. The above coupling frequencies can be written in terms of the appropriate Hopfield coefficients of the branches A_{ISPP}^U and A_{ISPP}^L [72] and the frequency $\bar{\Omega}_{S,A_{\text{bright}}}$ quantifying the coupling of the S_{SPP} mode with the intersubband bright excitation $P_{1,A}^{\text{MQW}}$. (Note that in contrast with the structures studied by Zhang *et al.* [72], only one of the effective oscillators, corresponding to the A_{ISPP}^L branch, can couple resonantly with the S_{SPP} oscillator. Moreover, due to the strong anisotropy of the intersubband excitation, the frequency separation between the "effective" oscillators A_{ISPP}^L and A_{ISPP}^U depends on $\bar{k}_x$.)

It is obvious that the spatial variation of the antisymmetric bright excitation $P_{1,A}^{\text{MQW}}$ does not coincide with the spatial variation of the symmetric bright excitation $P_{1,S}^{\text{MQW}}$. It means that the coupling frequency $\bar{\Omega}_{S,A_{\text{bright}}}$ is, in general, smaller than the coupling frequency $\bar{\Omega}_{R,S}$ defined by Eqs. (27) and (33). Nevertheless, we can expect that this difference is not substantial. It is connected with the fact that, at small $\bar{k}_x$, the coupling of S_{SPP} mode with branches A_{ISPP}^U and A_{ISPP}^L has a strongly nonresonant character. Consequently, this coupling rather weakly affects the characteristics of ISPP branches (located near and above $\bar{\omega}_{\text{IT}}$). On the other hand, when $\bar{k}_x$ increases, the difference between the spatial variation of the plasmonic mode functions $f_{A,z}$ and $f_{S,z}$ (in the region occupied by the MQW slab) decreases. It leads to the substantial reduction of the difference between coupling frequencies $\bar{\Omega}_{S,A_{\text{bright}}}$ and $\bar{\Omega}_{R,S}$. Thus, in the first approximation, we can neglect this difference.

Equation (35) predicts the origination, from the S_{SPP} and A_{SPP} modes, of not four but only three multimode polariton branches denoted by M_{ISPP}^U, M_{ISPP}^C, and M_{ISPP}^L. Their frequencies can be obtained solving the appropriate qubic equation resulting from (35) [72]. Unfortunately, the expressions for the frequencies of the above-mentioned branches are complex in general.

In further discussion, we employ the fact that in the considered now degenerate structures ($\bar{\omega}_A^{\text{cutoff}} = \bar{\omega}_{p,\text{mirr}}^{\text{surf}} = \bar{\omega}_{\text{IT}}$), $\bar{\omega}_A$ is very close to $\bar{\omega}_{\text{IT}}$ for arbitrary value of $\bar{k}_x$. It means that effective oscillators associated with the branches A_{ISPP}^U and A_{ISPP}^L have a nearly identical admixture of the plasmonic and intersubband components. In other words, we can take for

estimation $\bar{\Omega}_{S,A_{\mathrm{ISPP}}^L} \cong \bar{\Omega}_{S,A_{\mathrm{ISPP}}^U} \cong \bar{\Omega}_{R,A}/\sqrt{2}$. Moreover, we can employ the fact that when $\bar{k}_x$ is sufficiently large ($\gtrsim 2$), then the difference between $\bar{\omega}_S$ and $\bar{\omega}_A$ can be omitted. In this limit, the expression for the frequencies of the hybrid branches simplifies to the form

$$\bar{\omega}_{M_{\mathrm{ISPP}}^{U/L}} = \bar{\omega}_{\mathrm{IT}} \pm \sqrt{2}\bar{\Omega}_{R,A}, \quad \bar{\omega}_{M_{\mathrm{ISPP}}^C} = \bar{\omega}_{\mathrm{IT}}. \tag{36}$$

Thus, in the limit of large $\bar{k}_x$, the half of frequency splitting between branches M_{ISPP}^U and M_{ISPP}^L, supported by the degenerate structures, approaches $\sqrt{2}\bar{\Omega}_{R,A}$. The frequency of the central branch M_{ISPP}^C is then close to the intersubband frequency $\bar{\omega}_{\mathrm{IT}}$. It is worth to stress that Eq. (36) is consistent with the following general relation predicted by Eq. (35): $\bar{\omega}_{M_{\mathrm{ISPP}}^U} + \bar{\omega}_{M_{\mathrm{ISPP}}^C} + \bar{\omega}_{M_{\mathrm{ISPP}}^L} = \bar{\omega}_{A_{\mathrm{ISPP}}^U} + \bar{\omega}_{A_{\mathrm{ISPP}}^L} + \bar{\omega}_S$.

However, we should remember that the above conclusions are valid when the effects connected with the presence of the dark excitations ($P_{\mu',A}^{\mathrm{MQW}}$) are not considered. We know that the nonresonant coupling of the above dark excitations with higher (confined and nonconfined) resonator modes is responsible for the formation of the in-gap polariton branches. We know also that in the presently considered asymmetric structures, the single-mode approximation is violated. Thus, it is reasonable to expect that the behavior of the central branch M_{ISPP}^C should be additionally affected by its (resonant) coupling with the in-gap polaritons. Numerical results presented in Sec. VI are consistent with our suggestions.

V. MODE STRUCTURE OF PASSIVE RESONATORS

A. General considerations

The properties of the TM modes supported by passive (i.e., in the absence of the electronic excitation) plasmonic resonators have been extensively researched by many authors (see, e.g., [10–17,26,27]) in many different contexts. For example, in Refs. [13,15,16] the normal modes of lossless metal-dielectric-metal structures are studied in the context of the Casimir forces between metallic plates. On the other hand, many groups (see e.g., [14] and references therein) studied the mode structure of the subwavelength metal-dielectric-metal structures in the context of the application of the mode-matching technique to the analysis of metallic waveguides networks. It should be mentioned that in the latter case, the authors concentrate on propagation effects. For this reason, in [14], unlike in this paper and papers devoted to Casimir effect, modes with complex k_x are additionally considered.

As mentioned in the Introduction, in this paper we focus on the resonant coupling between the intersubband excitation and the (confined) plasmonic-type modes. Nevertheless, as already mentioned, the modal spectrum of the plasmonic resonators contains, in addition to the confined modes, also the continuous spectrum located above the boundary curve defined by Eq. (37). (This region is dark gray shaded in Figs. 2 and 3, where the eigenmodes of the passive resonators are displayed.) The continuous spectrum corresponds to the quantum-mechanical scattering states. The fields associated with such modes are finite at infinity. They are normalized by using the Dirac delta function. These modes play an essential role in the formation of in-gap polariton branches in plasmonic resonators. Numerical results reported in Sec. VI suggest that they are also responsible
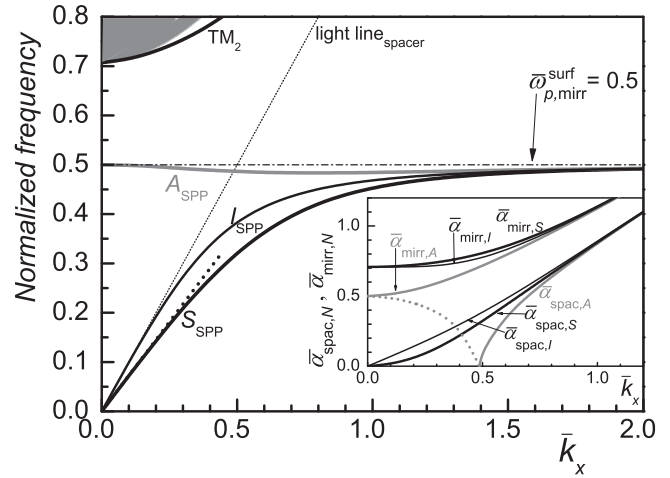

FIG. 2. The normalized frequencies of the modes S_{SPP}, A_{SPP}, I_{SPP} and TM_2 as a function of $\bar{k}_x$ (solid curves). For comparison, we also present results predicted by simplified Eq. (42) (black dotted line). The short-dotted (dashed-dotted) line corresponds to the spacer light line (the normalized surface plasma frequency $\bar{\omega}_{p,\mathrm{mirr}}^{\mathrm{surf}}$). The area located above the boundary curve $\bar{\alpha}_{\mathrm{mirr}} = 0$ is shaded. The inset displays $\bar{k}_x$ dependence of the parameters $\bar{\alpha}_{\mathrm{mirr/spac},N}$ corresponding to the modes S_{SPP} ($N = S$), A_{SPP} ($N = A$) and I_{SPP} ($N = I$). The dotted curves in the inset correspond to $\mathrm{Im}(\bar{\alpha}_{\mathrm{spac},A})$, $\bar{\omega}_{p,\mathrm{mirr}}^{\mathrm{surf}} = 0.5$.

for a non-negligible red-shift of the exact ISPP branches with respect to the results predicted by the single-mode secular equation (26). (We refer to [16] for detailed description of the properties of the continuous modes of the metal-dielectric-metal structure.)

To keep the discussion as self-contained as possible, in this section we summarize the essential information devoted to the dispersion characteristics of the S_{SPP} and A_{SPP} modes presented in the literature. Only the nondissipative characteristics are considered. We study also the behavior of the corresponding mode overlap factors $F_{S,z}$ and $F_{A,z}$. The above information will be employed in the next section for quasiparticle interpretation of the semiclassical dispersion characteristics predicted by Eqs. (12) and (11).
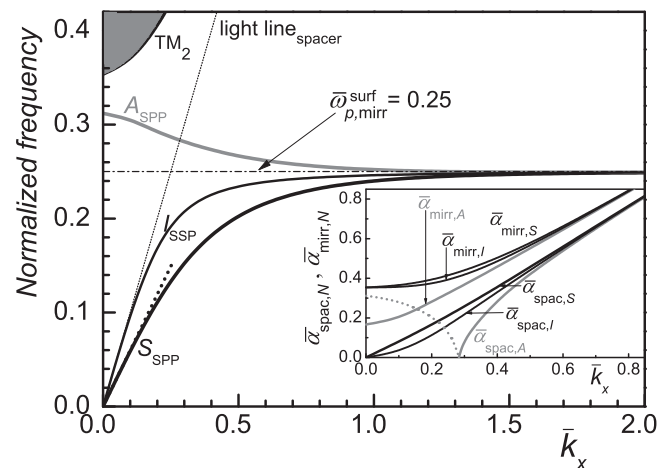

FIG. 3. Same as in Fig. 2, except that now $\bar{\omega}_{p,\mathrm{mirr}}^{\mathrm{surf}} = 0.25$.

We focus on the thin (subwavelength) resonators with $\bar{\omega}_{p,\mathrm{mirr}} \lesssim \bar{\omega}_{p,\mathrm{mirr}}^{\mathrm{crit}} \cong 0.84$ or, equivalently, with $\bar{\omega}_{p,\mathrm{mirr}}^{\mathrm{surf}} \lesssim 0.6$. It is motivated by the fact that only in such structures the negative dispersion of the A_{SPP} mode can be observed. Numerical calculations have been performed for the two types of lossless structures: with $\bar{\omega}_{p,\mathrm{mirr}}^{\mathrm{surf}} = 0.5$ (system I) and with $\bar{\omega}_{p,\mathrm{mirr}}^{\mathrm{surf}} = 0.25$ (system II). For convenience, it is assumed that (non-normalized) mirror plasma frequency $\omega_{p,\mathrm{mirr}}$ is the same in both systems. It means that the separation between mirrors in the system II is two times smaller than in the system I.

B. Surface- and oscillatory-type modes

The confined modes supported by the considered resonators are located (on the $\bar{\omega}$-$\bar{k}_x$ plane) below the boundary curve [13–16]

$$\bar{\omega}_{\mathrm{bound}}(\bar{k}_x) = \left(\bar{\omega}_{p,\mathrm{mirr}}^2 + \bar{k}_x^2\right)^{1/2}, \tag{37}$$

resulting from the condition $\bar{\alpha}_{\mathrm{mirr}}(\bar{\omega},\bar{k}_x) = 0$. Only such modes have evanescent tails ($\bar{\alpha}_{\mathrm{mirr}}$ is real) within the plasmonic claddings.

We divide the area under the boundary curve (37) into two regions denoted by $\mathcal{W}_{\mathrm{spac}}$ and $\mathcal{S}_{\mathrm{spac}}$. The region $\mathcal{W}_{\mathrm{spac}}$ ($\mathcal{S}_{\mathrm{spac}}$) is positioned within (outside) the spacer light cone defined by the spacer light line $\bar{\omega} = \bar{k}_x$. In the region $\mathcal{W}_{\mathrm{spac}}$ ($\mathcal{S}_{\mathrm{spac}}$) the quantity $\bar{\alpha}_{\mathrm{spac}}$ is imaginary (real). It means that the eigenmodes located in the region $\mathcal{S}_{\mathrm{spac}}$ are surface-type modes while the eigenmodes located in the region $\mathcal{W}_{\mathrm{spac}}$ are (ordinary) waveguide/oscillatory-type modes.

C. Characteristics of single-interface SPP mode

At first, we briefly discuss the properties of single-interface surface plasmon polariton mode denoted by I_{SPP}. This mode obeys the following dispersion equation:

$$\bar{\alpha}_{\mathrm{mirr}}/\bar{\alpha}_{\mathrm{spac}} = -\varepsilon_{\mathrm{mirr}}/\varepsilon_w. \tag{38}$$

This equation results from Eq. (12) when the separation between mirrors is sufficiently large or, more precisely, when the coupling between the single-interface modes is small. Such situation takes place when the condition $\alpha_{\mathrm{spac},I} L_{\mathrm{MC}} < 1$ is fulfilled (see below). The above condition can be equivalently written as $\bar{\alpha}_{\mathrm{spac},I} > \bar{\alpha}^* = 1/\pi \cong 0.32$ where $\bar{\alpha}_{\mathrm{spac},I} \equiv \bar{\alpha}_{\mathrm{spac}}(\omega_I)$.

The normalized frequency $\bar{\omega}_I$ $(=\omega_I/\omega_\perp)$ of the I_{SPP} mode, predicted by Eq. (38), is given by [15,73]

$$\bar{\omega}_I(\bar{k}_x) = \sqrt{\left(\bar{\omega}_{p,\mathrm{mirr}}^{\mathrm{surf}}\right)^2 + \bar{k}_x^2 - \sqrt{\left(\bar{\omega}_{p,\mathrm{mirr}}^{\mathrm{surf}}\right)^4 + \bar{k}_x^4}}. \tag{39}$$

The $\bar{k}_x$ dependence of $\bar{\omega}_I$ is presented in Figs. 2 and 3 by thin solid curves. As one can expect, the I_{SPP} mode is located in the $\mathcal{S}_{\mathrm{spac}}$ region, i.e., it has a surface character. It starts linearly $[\bar{\omega}_I(\bar{k}_x) \cong \bar{k}_x]$ at $(\bar{\omega} = 0, \bar{k}_x = 0)$ and goes asymptotically towards $\bar{\omega}_{p,\mathrm{mirr}}^{\mathrm{surf}}$ as $\bar{k}_x \to \infty$.

D. Characteristics of coupled SPP modes

When the coupling between single-interface SPP modes is small, then it is reasonable to expect that, like in the case of the coupled semiconductor resonators [42], the two-coupled-

oscillator model can be employed. It means that the frequencies of the symmetric and antisymmetric plasmonic modes can be approximated by

$$\bar{\omega}_{A/S} = \bar{\omega}_I(1 \pm \kappa_I). \tag{40}$$

The expression for the $\bar{k}_x$-dependent coupling factor κ_I can be obtained employing a formalism developed in Ref. [71]. This formalism is similar to the tight-binding method in solid-state physics. As one can expect, obtained in this way the coupling factor is proportional to $(\exp - \alpha_{\mathrm{spac},I} L_{\mathrm{MC}})$. (Details will be presented in a future paper.) The described above simplification will be an important point in a subsequent discussion in Appendix D concerning the interpretation of the polariton-induced optical asymmetry observed in the four-layer structures.

Making in Eq. (12) the replacement $\alpha_{\mathrm{MQW}} \to \alpha_{\mathrm{spac}}$ one finds that the characteristic equation describing the TM modes supported by the passive resonator (with arbitrary thickness) can be written in the following dimensionless form:

$$\tanh(\bar{\alpha}_{\mathrm{spac}}\pi/2) = -(\bar{\alpha}_{\mathrm{mirr}}\varepsilon_w/\varepsilon_{\mathrm{mirr}}\bar{\alpha}_{\mathrm{spac}})^{\pm 1}. \tag{41}$$

The number of bound modes (n_{bound}) resulting from this equation depends on the dimensionless plasma frequency: $n_{\mathrm{bound}} = [\bar{\omega}_{p,\mathrm{mirr}}/2] + [(\bar{\omega}_{p,\mathrm{mirr}} + 1)/2] + 3$ (see Refs. [10,16]). (The brackets indicate the integer part of the number.) Thus, sub-wavelength resonators with $\bar{\omega}_{p,\mathrm{mirr}} = \sqrt{2} \times 0.5 \cong 0.71$ (the system I) and $\bar{\omega}_{p,\mathrm{mirr}} = \sqrt{2} \times 0.25 \cong 0.35$ (the system II) considered in this paper support only three modes: two plasmonic-type modes (S_{SPP} and A_{SPP}) and one photonic-type mode (TM$_2$). The dispersion characteristics of the modes supported by the systems I and II are displayed in Figs. 2 and 3, respectively. These figures show that the photonic TM$_2$ mode starts at the frequency slightly smaller than $\bar{\omega}_{p,\mathrm{mirr}}$ and is located (for all values of $\bar{k}_x$) in the $\mathcal{W}_{\mathrm{spac}}$ region, slightly below the boundary curve. The properties of this oscillatory-type mode are not discussed in this paper. Some details on its behavior can be found in Refs. [10,33]. In this section we focus on the S_{SPP} and A_{SPP} modes.

1. The S_{SPP} mode

The S_{SPP} mode is located below the I_{SPP} mode in the region $\mathcal{S}_{\mathrm{spac}}$ for all values of $\bar{k}_x$. Like the I_{SPP} mode, it starts at $(\bar{k}_x = 0, \bar{\omega} = 0)$ and goes asymptotically towards $\bar{\omega}_{p,\mathrm{mirr}}^{\mathrm{surf}}$ when $\bar{k}_x \to \infty$. At small $\bar{k}_x$ one gets the linear dispersion [13]

$$\bar{\omega}_S(\bar{k}_x) = \bar{k}_x/\sqrt{1 + 2/(\pi \bar{\omega}_{p,\mathrm{mirr}})}. \tag{42}$$

The $\bar{k}_x$ dependence of the S_{SPP} mode predicted by Eqs. (41) and (42) is represented in Figs. 2 and 3 by black solid and black dotted curves, respectively. We find that in the case of the structure with $\bar{\omega}_{p,\mathrm{mirr}}^{\mathrm{surf}} = 0.5$ ($\bar{\omega}_{p,\mathrm{mirr}}^{\mathrm{surf}} = 0.25$), Eq. (42) works very well at $\bar{k}_x \lesssim 0.4$ ($\bar{k}_x \lesssim 0.25$). We find also that the difference between the modes I_{SPP} and S_{SPP} increases with decreasing $\bar{\omega}_{p,\mathrm{mirr}}^{\mathrm{surf}}$ and, in the considered structures, is noticeable for $\bar{k}_x \lesssim 1$.

2. The A_{SPP} mode

The behavior of the dispersion curve $\bar{\omega}_A$ of the A_{SPP} mode is more complex than the S_{SPP} and I_{SPP} modes. Namely, the
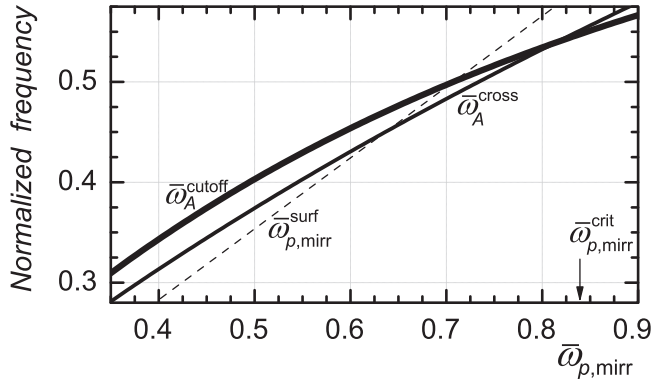
FIG. 4. The $\bar{\omega}_{p,\text{mirr}}$ dependence of the normalized cutoff frequency $\bar{\omega}_A^{\text{cutoff}}$ (thick solid line) and the normalized crossing frequency $\bar{\omega}_A^{\text{cross}}$ (thin solid line). The dashed line corresponds to the normalized surface plasmon frequency $\bar{\omega}_{p,\text{mirr}}^{\text{surf}}$.

A_{SPP} mode, in contrast with the above-mentioned modes, starts at ($\bar{k}_x = 0$, $\bar{\omega} = \bar{\omega}_A^{\text{cutoff}} \neq 0$), i.e., in the region $\mathcal{W}_{\text{spac}}$, as an oscillatory-type mode (see dark gray curves in Figs. 2 and 3). From Eqs. (41) and (17), one finds that the normalized cutoff frequency $\bar{\omega}_A^{\text{cutoff}} \equiv \bar{\omega}_A(\bar{k}_x = 0)$ satisfies the following relation:

$$\bar{\omega}_A^{\text{cutoff}} = \frac{2}{\pi} \arctan\left\{\left[\left(\bar{\omega}_{p,\text{mirr}}/\bar{\omega}_A^{\text{cutoff}}\right)^2 - 1\right]^{1/2}\right\}. \quad (43)$$

The results predicted by this equation are presented in Fig. 4 as a thick solid curve. This figure illustrates our previous statement that $\bar{\omega}_A^{\text{cutoff}} > \bar{\omega}_{p,\text{mirr}}^{\text{surf}}$ ($\bar{\omega}_A^{\text{cutoff}} < \bar{\omega}_{p,\text{mirr}}^{\text{surf}}$) when $\bar{\omega}_{p,\text{mirr}}^{\text{surf}} > 0.5$ ($\bar{\omega}_{p,\text{mirr}}^{\text{surf}} < 0.5$).

Employing appropriate expansions (see [19,74]) one can check that at $\bar{k}_x \ll 1$, the dispersion curve $\bar{\omega}_A(\bar{k}_x)$ is a parabola with vertex at $\bar{k}_x = 0$. Thus, we can speak about the formation of ZGV point at $\bar{k}_x = 0$. Depending on the value of $\bar{\omega}_{p,\text{mirr}}$, the parabola is upwardly or downwardly concave. The critical value of the mirror plasma frequency ($\bar{\omega}_{p,\text{mirr}}^{\text{crit}}$) at which the dispersion curvature of $\bar{\omega}_A(\bar{k}_x)$ changes its sign obeys the following relation [74]:

$$\left(\bar{\omega}_{p,\text{mirr}}^{\text{crit}}\right)^2 = \left(\bar{\omega}_A^{\text{cutoff}}\right)^2 + (2/\pi)^2. \quad (44)$$

Substituting (44) into (43) we get an equation for $\bar{\omega}_{p,\text{mirr}}^{\text{crit}}$. The numerical solution of this equation gives $\bar{\omega}_{p,\text{mirr}}^{\text{crit}} \cong 0.854$. We have obtained a slightly smaller value of $\bar{\omega}_{p,\text{mirr}}^{\text{crit}} (\cong 0.840)$ solving numerically Eq. (41) for different values of $\bar{\omega}_{p,\text{mirr}}$. The latter result coincides with the result reported in Ref. [10].

The dispersion curve $\bar{\omega}_A(\bar{k}_x)$ crosses the spacer light line at $\bar{\omega} = \bar{\omega}_A^{\text{cross}}$ given by [10,13,15,74]

$$\bar{\omega}_A^{\text{cross}} = \bar{\omega}_{p,\text{mirr}}/\sqrt{1 + \bar{\omega}_{p,\text{mirr}}\pi/2}. \quad (45)$$

It is obvious that at the crossing point ($\bar{k}_x = \bar{k}_A^{\text{cross}}$, $\bar{\omega} = \bar{\omega}_A^{\text{cross}}$) the antisymmetric mode changes its character from the oscillatory type into the surface type. Near this point, the A_{SPP} mode is linearly dispersive and the normal component of the electric field connected with the above mode changes linearly with z (i.e., $E_{A,z} \sim z$) [74].

The dependence of $\bar{\omega}_A^{\text{cross}}$ on $\bar{\omega}_{p,\text{mirr}}$, predicted by Eq. (45), is displayed in Fig. 4 as a thin solid line. We find that at
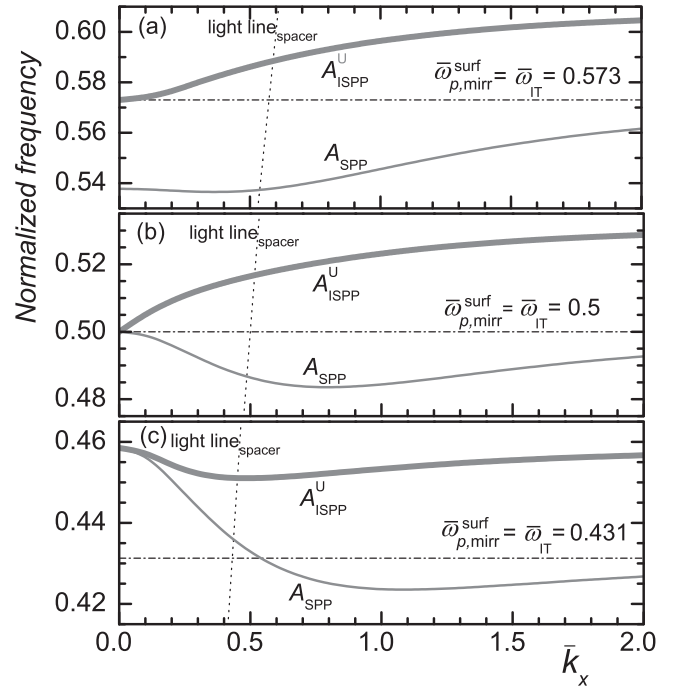

FIG. 5. The normalized frequencies of the A_{SPP} mode and the A_{ISPP}^U polariton branch supported by the three-layer structures, with different values of $\bar{\omega}_{p,\text{mirr}}^{\text{surf}} = \bar{\omega}_{\text{IT}}$, as a function of $\bar{k}_x$. The short-dotted (dashed-dotted) line corresponds to the light line (the normalized frequency $\bar{\omega}_{p,\text{mirr}}^{\text{surf}} = \bar{\omega}_{\text{IT}}$). $\bar{\varpi}_{p,\text{MQW}} = 0.3 \times \bar{\omega}_{\text{IT}}$.

$\bar{\omega}_{p,\text{mirr}} \cong 0.81$ (or equivalently at $\bar{\omega}_{p,\text{mirr}}^{\text{surf}} \cong 0.573$) the crossing frequency coincides with cutoff frequency ($\bar{\omega}_A^{\text{cross}} = \bar{\omega}_A^{\text{cutoff}} \cong 0.54$). It means that in the structures with $\bar{\omega}_{p,\text{mirr}}$ close to 0.81 the antisymmetric mode can be treated (at $\bar{k}_x \leqslant \bar{k}_A^{\text{cross}} \cong 0.54$) as effectively quasi-dispersionless. This situation is illustrated in Fig. 5(a). It is consistent with the experimental results reported in Ref. [19].

As mentioned, at $\bar{k}_x \to \infty$ the A_{SPP} mode goes asymptotically, always from a low-frequency side, towards $\bar{\omega}_{p,\text{mirr}}^{\text{surf}}$ [18]. It means that in sufficiently thin resonators ($\bar{\omega}_{p,\text{mirr}} \leqslant \bar{\omega}_{p,\text{mirr}}^{\text{crit}} \cong 0.840$) the formation, at finite $\bar{k}_x (=\bar{k}_A^{\text{min}})$, of a shallow minimum in the dispersion curve $\bar{\omega}_A$ takes place [10,18]. The normalized depth of the above-mentioned minimum $\bar{\delta}_{\text{depth}} = [\bar{\omega}_{p,\text{mirr}}^{\text{surf}} - \bar{\omega}_A(\bar{k}_A^{\text{min}})]/\bar{\omega}_{p,\text{mirr}}^{\text{surf}}$ takes the largest value ($\cong 0.032$) when $\bar{\omega}_{p,\text{mirr}}^{\text{surf}} = 0.5$. It is located at $\bar{k}_x = \bar{k}_A^{\text{min}} \cong 0.8$. For comparison, in the thinner structures ($\bar{\omega}_{p,\text{mirr}}^{\text{surf}} = 0.25$) the minimum of the curve $\bar{\omega}_A(\bar{k}_x)$ is shifted to $\bar{k}_A^{\text{min}} \approx 2$ and its normalized depth $\bar{\delta}_{\text{depth}}$ reduces to the negligibly small value of 0.004. The inspection of the numerical results displayed in Figs. 2 and 3 (see also Fig. 5) clearly shows that when the difference $|\bar{\omega}_{p,\text{mirr}}^{\text{surf}} - 0.5|$ increases, then $\bar{\delta}_{\text{depth}}$ decreases while $\bar{k}_x^{\text{min}}$ increases. (As mentioned, the minimum in the curve $\bar{\omega}_A$ appears only when $\bar{\omega}_{p,\text{mirr}} < \bar{\omega}_{p,\text{mirr}}^{\text{crit}} \cong 0.84$.)

3. Penetration depth inside mirror and spacer regions

The z component of the electric field connected with the Nth mode ($E_{N,z}$) takes the maximal value at the $\varepsilon_{\text{mirr}}|\varepsilon_{\text{spac}}$ interfaces (see Appendix B). Thus, the quantities $\alpha_{\upsilon,N}^{-1} \equiv$
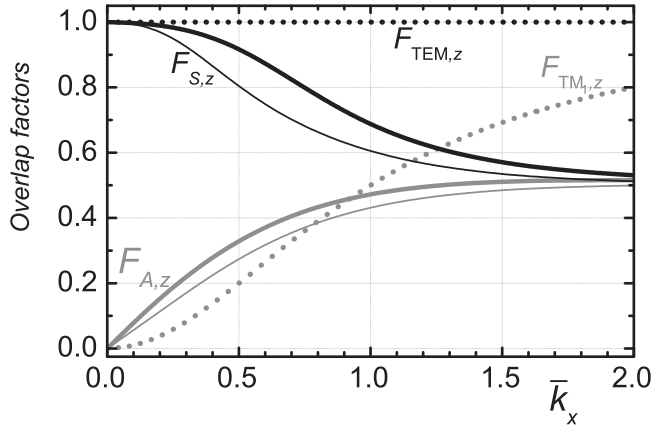
FIG. 6. The thick (thin) solid curves present the $\bar{k}_x$ dependence of the overlap factors corresponding to the modes S_{SPP} and A_{SPP} supported by resonator with $\bar{\omega}_{p,\text{mirr}}^{\text{surf}} = 0.5$ ($\bar{\omega}_{p,\text{mirr}}^{\text{surf}} = 0.25$). For comparison, we present also the $\bar{k}_x$ dependence of the overlap factors corresponding to the modes $\text{TM}_0 \equiv \text{TEM}$ and TM_1 supported by the resonators with perfect metallic mirrors (the dotted curves).

$\alpha_v^{-1}(\omega_N)$, defined by Eqs. (14) and (15), can be considered as penetration depth inside the $v = \text{mirr,spac}$ region of the S_{SPP} ($N = S$), A_{SPP} ($N = A$), or I_{SPP} ($N = I$) mode.

The $\bar{k}_x$ variation of the normalized penetration depth $\bar{\alpha}_{v,N}$, for the systems I and II present the insets in Figs. 2 and 3, respectively. For convenience, in the range of small $\bar{k}_x$, where $\bar{\alpha}_{\text{spac},A}$ is imaginary, we display the behavior of $\text{Im}(\bar{\alpha}_{\text{spac},A})$.

As mentioned, the coupling between the single-interface modes is small when $\bar{\alpha}_{\text{spac},I}$ is larger than $\bar{\alpha}^*$ ($\cong 0.32$). The inspection of Figs. 2 and 3 shows that in our structures, the above condition is fulfilled only at relatively large values of $\bar{k}_x$ ($\gtrsim 0.5$). Moreover, as one can expect, at large $\bar{k}_x$ ($\gtrsim 1$) the dependence of $\bar{\alpha}_{v,N}$ on the mode index N is rather weak.

E. Plasmonic mode overlap factors

Now, we discuss the behavior of the mode overlap factors $F_{S,z}$ and $F_{A,z}$ defined by Eq. (33). The factor $F_{\mathcal{N},z}$ controls the coupling strength of the $\mathcal{N}$th plasmonic mode with the intersubband bright excitation $P_{1,\mathcal{N}}^{\text{MQW}}$. The explicit expressions for the above factors are given in Appendix C [see Eqs. (C1)–(C6)]. Unfortunately, the presence of the hyperbolic functions in these equations makes their analysis by analytic methods rather impossible. That is why we performed numerical calculations. Figure 6 displays the results of these calculations for the systems studied in Figs. 2 and 3. For comparison, we also display the $\bar{k}_x$ dependence of the overlap factors $F_{\text{TEM},z}$ ($F_{\text{TM}_1,z}$) corresponding to the TEM $= \text{TM}_0$ (TM_1) modes supported by the structures with perfect metallic mirrors [see Eq. (25)].

We observe that the behavior of the overlap factors strongly depends on the mode index. In the idealized case of perfect metallic mirrors, the factor $F_{\text{TEM},z}$ is constant ($F_{\text{TEM},z} = 1$) while the factor $F_{\text{TM}_1,z}$ increases with $\bar{k}_x$ from 0 to its asymptotic value of 1 according to Eq. (25). The above dependence is a consequence of the strong anisotropy of the intersubband excitations. The replacement of perfect metal boundary conditions by realistic ones introduces a substantial modification in the behavior of the overlap factors. It is easy

to see that now, in contrast with the idealized case, both factors $F_{S,z}$ and $F_{A,z}$ are the monotonous functions of $\bar{k}_x$. However, the factor $F_{S,z}$ decreases from its maximal value of 1 at $k_x = 0$ to the asymptotic value of $\frac{1}{2}$ in the limiting case of large $\bar{k}_x$ ($\gtrsim 2$). It is worth stressing that, when the structure is not too thin (more precisely when $\bar{\omega}_{p,\text{mirr}} \gtrsim 1$), then the penetration of the S_{SPP} mode into the mirrors very weakly affects the mode factor $F_{S,z}$ in the range of the small $\bar{k}_x$. Equivalently, we can say that in the above-mentioned limit, the replacement of the perfect mirrors by realistic plasmonic mirrors affects practically only the mode frequency $\bar{\omega}_S$. (This finding is consistent with suggestion reported in Ref. [5].) The behavior of the factor $F_{A,z}$ is different. It increases from its minimal value of 0 at $\bar{k}_x = 0$ to the asymptotic value of $\frac{1}{2}$. Note, however, that in contrast with the factors $F_{S,z}$ and $F_{\text{TEM},z}$, the difference between the factors $F_{A,z}$ and $F_{\text{TM}_1,z}$ is negative at large $\bar{k}_x$ but positive (and non-negligible) at small $\bar{k}_x$.

The fact that the factors $F_{S,z}$ and $F_{A,z}$ approach the same asymptotic value of $\frac{1}{2}$ can be explained in the following way. At large $\bar{k}_x$ ($\gtrsim 2$) the modes S_{SPP} and A_{SPP} practically transform into the (symmetric and antisymmetric) combination of the single-interface modes. Simultaneously, their frequencies approach $\bar{\omega}_{p,\text{mirr}}^{\text{surf}}$. At $\bar{\omega}$ close to $\bar{\omega}_{p,\text{mirr}}^{\text{surf}}$, the ratio $-\varepsilon_{\text{mirr}}/\varepsilon_{\text{spac}}$ is close to unity and the relation $\bar{\alpha}_{\text{mirr/spac},\mathcal{N}} \cong \bar{k}_x$ is approximately valid. From the former relation we find that, not only $|E_{\mathcal{N},x}|^2$ but also $|E_{\mathcal{N},z}|^2$ appearing in Eq. (33) for the mode overlap factor can be treated as continuous across the interfaces $\varepsilon_{\text{mirr}}|\varepsilon_{\text{spac}}$. Simultaneously, the relation $\bar{\alpha}_{\text{mirr/spac},\mathcal{N}} \cong \bar{k}_x$ implies that $|E_{\mathcal{N},z}|^2 \cong |E_{\mathcal{N},x}|^2$ in the mirrors as well as in the spacer layer (see Appendix B). Taking into account the above simplifications, one finds from Eq. (33) that $F_{S,z} \cong F_{A,z} \cong 1/2$ at $\bar{k}_x \gtrsim 2$.

VI. MODE CHARACTERISTICS OF RESONATORS WITH EMBEDDED MQW

Now, we turn our attention to the main subject of this paper: the discussion of the properties of the ISPP branches supported by the three- and four-layer structures. Only confined electromagnetic modes, i.e., the modes located below the mirror boundary curve [see Eq. (37)] will be considered. Moreover, similarly to the previous section, we completely neglect dissipative losses. It is well known that such simplification works well when the structure exhibits a strong coupling regime, i.e., when $\Omega_{R,\mathcal{N}} > \gamma_{\text{IT}}, \gamma_{\mathcal{N}}$, where γ_{IT} ($\gamma_{\mathcal{N}}$) is the decay rate of the intersubband excitation (the $\mathcal{N}$th plasmonic mode). We have validated this approximation showing in Appendix D that, to a large extent, the lossless characteristics of the ISPP branches are consistent with the angle-resolved reflection-absorption spectra of the GaAlAs-based realistic structures. Additionally, we demonstrate that the dispersion characteristics of the ISPPs resulting from the semiclassical equations (12) and (11) are consistent with the quasiparticle picture. The possibility of the engineering of these characteristics (mainly in the context of the slow/stopped light effects) will be also discussed.

To facilitate the comparison of the characteristics of the three- and four-layer structures, we assume that the period (d_{MQW}) of the MQW slab, located in the four-layer structure, is two times smaller than the period of the MQW slab located
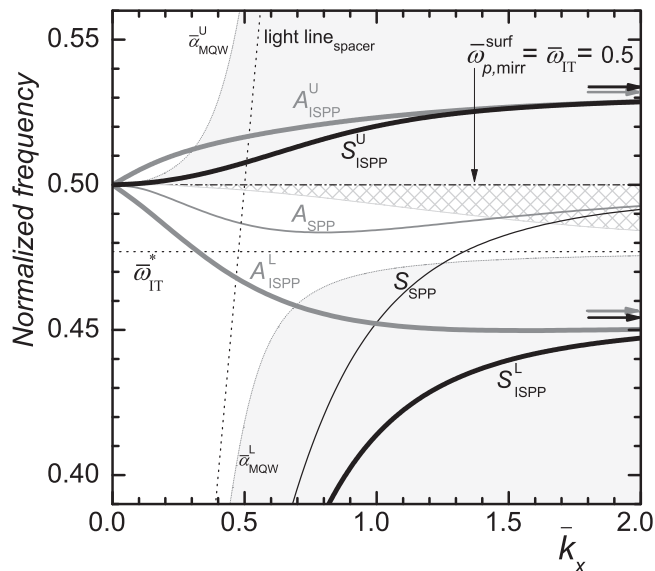
FIG. 7. The normalized frequencies of the ISPP branches supported by the three-layer structure as a function of $\bar{k}_x$ (the thick solid curves). For illustration, the normalized frequencies of the plasmonic modes supported by the passive structure are also displayed (the thin solid curves). The short-dotted (dashed-dotted) line corresponds to the light line (the normalized intersubband frequency $\bar{\omega}_{\mathrm{IT}}$ and surface plasma frequency $\bar{\omega}_{p,\mathrm{mirr}}^{\mathrm{surf}}$). The interpretation of the black and gray horizontal arrows is given in the main text. The area where in-gap intersubband polariton branches are located is hatched. The regions $\mathcal{S}_{\mathrm{MQW}}^U$ and $\mathcal{S}_{\mathrm{MQW}}^L$ where the intersubband polariton branches have surface character are light gray shaded. $\bar{\omega}_{p,\mathrm{mirr}}^{\mathrm{surf}} = \bar{\omega}_{\mathrm{IT}} = 0.5$ and $\bar{\varpi}_{p,\mathrm{MQW}} = 0.3 \times \bar{\omega}_{\mathrm{IT}}$.

FIG. 8. Same as in Fig. 7, except that now $\bar{\omega}_{p,\mathrm{mirr}}^{\mathrm{surf}} = \bar{\omega}_{\mathrm{IT}} = 0.25$. Moreover, for illustration we present additionally the dispersion of the branches A_{ISPP}^U and A_{ISPP}^L obtained employing Eq. (26) (open circles).

in the three-layer structure ($d_{\mathrm{MQW}}^{\mathrm{three\text{-}layer}} = 2d_{\mathrm{MQW}}^{\mathrm{four\text{-}layer}}$). Other parameters of the MQWs and the cladding materials are identical. Moreover, performing the numerical calculations we assume that in the case of the three-layer structure $\bar{\varpi}_{p,\mathrm{MQW}} = 0.3 \times \bar{\omega}_{\mathrm{IT}}$. The above-mentioned assumptions imply that in the four-layer structure $\bar{\varpi}_{p,\mathrm{MQW}} = \sqrt{2} \times (0.3 \times \bar{\omega}_{\mathrm{IT}})$. As mentioned, we focus mainly on the degenerate structures ($\bar{\omega}_{\mathrm{IT}} = \bar{\omega}_{p,\mathrm{mirr}}^{\mathrm{surf}} = \bar{\omega}_A^{\mathrm{cutoff}}$). It is connected with the fact that in such structures the A_{SPP} mode is nearly resonant with intersubband transitions for arbitrary $\bar{k}_x$ while the S_{SPP} mode becomes nearly resonant only at large value of $\bar{k}_x$ ($\gtrsim 1$).

A. Three-layer structures

We start from the discussion of the three-layer (symmetric) structures. The ISPP branches resulting from the characteristic equation (12) have the surface or oscillating character depending on the sign of $\bar{\alpha}_{\mathrm{MQW}}^2$ defined by Eq. (16). Let us denote by $\bar{\alpha}_{\mathrm{MQW}}^U$ ($\bar{\alpha}_{\mathrm{MQW}}^L$) the upper (lower) solution of the equation $\bar{\alpha}_{\mathrm{MQW}}(\bar{\omega}, \bar{k}_x) = 0$. Numerical simulations show (see Figs. 7 and 8) that the lower solution $\bar{\alpha}_{\mathrm{MQW}}^L$ starts linearly at ($\bar{k}_x = 0$, $\bar{\omega} = 0$) and goes asymptotically towards $\bar{\omega}_{\mathrm{IT}}^*$ as $\bar{k}_x \to \infty$. The upper solution $\bar{\alpha}_{\mathrm{MQW}}^U$ starts at ($\bar{k}_x = 0$, $\bar{\omega} = \bar{\omega}_{\mathrm{IT}}$) and approaches asymptotically the spacer light line $\bar{\alpha}_{\mathrm{spac}}(\omega) = 0$ as $\bar{k}_x \to \infty$.

For further discussion, it is convenient to divide the $\bar{k}_x$-$\bar{\omega}$ plane, located below the mirror boundary curve [defined
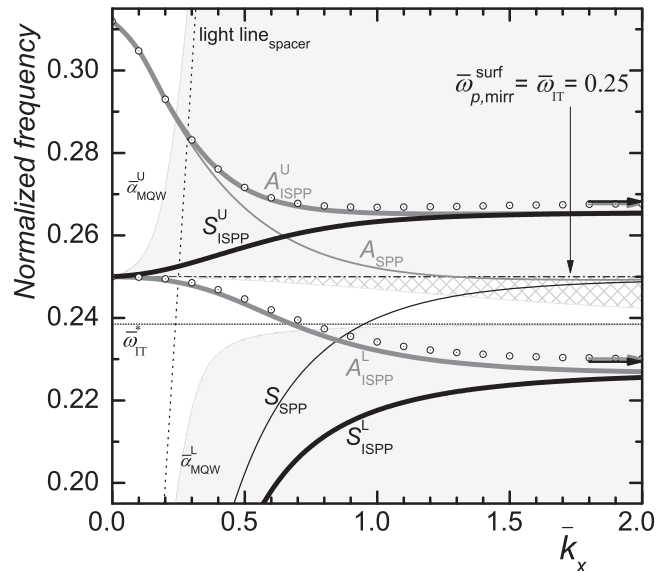
Eq. (37)] into four regions denoted by $\mathcal{W}_{\mathrm{MQW}}^U$, $\mathcal{S}_{\mathrm{MQW}}^U$, $\mathcal{W}_{\mathrm{MQW}}^L$, and $\mathcal{S}_{\mathrm{MQW}}^L$. The region $\mathcal{W}_{\mathrm{MQW}}^U$ ($\mathcal{S}_{\mathrm{MQW}}^L$) is positioned above (below) the branch $\bar{\alpha}_{\mathrm{MQW}}^U$ ($\bar{\alpha}_{\mathrm{MQW}}^L$) while the region $\mathcal{S}_{\mathrm{MQW}}^U$ ($\mathcal{W}_{\mathrm{MQW}}^L$) is located between horizontal line $\bar{\omega} = \bar{\omega}_{\mathrm{IT}}$ and branch $\bar{\alpha}_{\mathrm{MQW}}^U$ ($\bar{\alpha}_{\mathrm{MQW}}^L$). (In Figs. 7 and 8, the regions $\mathcal{S}_{\mathrm{MQW}}^U$ and $\mathcal{S}_{\mathrm{MQW}}^L$ are light gray shaded.) Inside the regions $\mathcal{S}_{\mathrm{MQW}}^U$ and $\mathcal{S}_{\mathrm{MQW}}^L$ ($\mathcal{W}_{\mathrm{MQW}}^U$ and $\mathcal{W}_{\mathrm{MQW}}^L$) the quantity $\bar{\alpha}_{\mathrm{MQW}}$ is real (imaginary). It means that the polariton branches located inside (outside) regions $\mathcal{S}_{\mathrm{MQW}}^U$ and $\mathcal{S}_{\mathrm{MQW}}^L$ can be treated as surface (waveguide/oscillating-) type modes.

1. Nondegenerate structures

It is instructive to start discussion from typical nondegenerate structures with metallic mirrors (see, e.g., [4]) where $\bar{\omega}_{\mathrm{IT}}$ is substantially smaller than $\bar{\omega}_{p,\mathrm{mirr}}^{\mathrm{surf}}$. In such structures, only the S_{SPP} mode couples resonantly with intersubband transitions ($n_{\mathrm{res}} = S$). Figure 9 presents the anticrossing behavior of the S_{ISPP}^U and S_{ISPP}^L branches at $\bar{k}_x$ close to the resonant value $\bar{k}_S^{\mathrm{res}}$ (at which $\bar{\omega}_S = \bar{\omega}_{\mathrm{IT}}$). Results displayed in Fig. 9(a) [9(b)] are obtained for the structure with $\bar{\omega}_{p,\mathrm{mirr}}^{\mathrm{surf}} = 0.5$ and $\bar{\varpi}_{p,\mathrm{MQW}} = 0.3 \times \bar{\omega}_{\mathrm{IT}}$, taking $\bar{\omega}_{\mathrm{IT}} = 0.1$ ($\bar{\omega}_{\mathrm{IT}} = 0.4$). The thick solid curves represent the exact results predicted by Eq. (12). The open circles are obtained employing the generalized secular equation [see Eqs. (26) and (27)] based on the single-mode cavity approximation. As one can expect, when the ratio $\bar{\omega}_{\mathrm{IT}}/\bar{\omega}_{p,\mathrm{mirr}}^{\mathrm{surf}}$ is small ($\lesssim 0.2$), then Eqs. (26) and (27) very well reproduce the exact results even if we take $F_{S,z} = F_{\mathrm{TEM},z} = 1$ (results are not presented). However, when, like in Fig. 9(b), the ratio $\bar{\omega}_{\mathrm{IT}}/\bar{\omega}_{p,\mathrm{mirr}}^{\mathrm{surf}}$ is close to unity (=0.8), the $\bar{k}_x$ dependence of the factor $F_{S,z}$ (see Fig. 6) starts to play an important role. For example, taking $F_{S,z} = 1$ we get the overestimated (by about 16%) value of the polariton branch splitting (at $\bar{k}_x = \bar{k}_S^{\mathrm{res}}$) in the case of the structure discussed in Fig. 9(b).
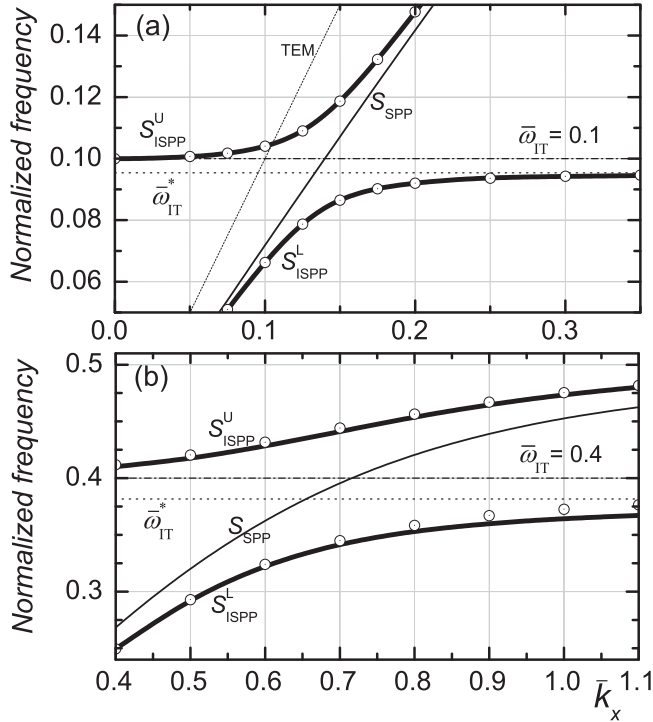
FIG. 9. The normalized frequencies of the branches $S_{\rm ISPP}^{U}$ and $S_{\rm ISPP}^{L}$ supported by the nondegenerate structures as a function of $\bar{k}_x$. Thick solid curves represent exact results predicted by Eq. (12). Open circles are obtained employing the generalized secular equation (26) based on the single-mode cavity approximation. Thin solid (dashed) curves represent $\bar{k}_x$ dependence of the $S_{\rm SPP}$ (TEM) mode. Calculations have been performed taking (a) $\bar{\omega}_{\rm IT} = 0.1$ and (b) $\bar{\omega}_{\rm IT} = 0.4$. $\bar{\omega}_{p,\rm mirr}^{\rm surf} = 0.5$ and $\bar{\varpi}_{p,\rm MQW} = 0.3 \times \bar{\omega}_{\rm IT}$.

It is worth stressing that even if we include the $\bar{k}_x$ dependence of the factor $F_{S,z}^{-}$ we are not able to reproduce precisely the exact results predicted by Eq. (12). A small, but non-negligible red-shift of the exact results (mainly lower branch) with respect to the results predicted by the single-mode cavity approximation (26) appears at $\bar{k}_x \gtrsim 1$. A similar effect has been predicted in our previous paper [37] for the semiconductor MC-QW structure. We will return to this problem at the end of this section.

2. Degenerate structures

Now, we discuss the characteristics of the ISPP branches supported by the degenerate structure ($\bar{\omega}_{\rm IT} = \bar{\omega}_{p,\rm mirr}^{\rm surf} = 0.5$) and nearly degenerate structure ($\bar{\omega}_{\rm IT} = \bar{\omega}_{p,\rm mirr}^{\rm surf} = 0.25$). (We remind that only in the case of the degenerate structure the condition $\bar{\omega}_{\rm IT} = \bar{\omega}_{p,\rm mirr}^{\rm surf} = \bar{\omega}_{p,\rm mirr}^{\rm cutoff}$ is fulfilled.) The dispersion characteristics of the above mentioned structures are displayed in Figs. 7 and 8. In agreement with the quasiparticle picture, aside from the $S_{\rm ISPP}^{U/L}$ and $A_{\rm ISPP}^{U/L}$ branches, originating from the $S_{\rm SPP}$ and $A_{\rm SPP}$ plasmonic modes, the characteristic equation (12) predicts the formation of the in-gap intersubband polariton branches.

a. Symmetric ISPP branches. The results displayed in Figs. 7 and 8 show that the symmetric branches $S_{\rm ISPP}^{U}$ and $S_{\rm ISPP}^{L}$ are located in the regions $\mathcal{S}_{\rm MQW}^{L}$ and $\mathcal{S}_{\rm MQW}^{U}$, respectively. It

means that they have a surface character. The upper branch $S_{\rm ISPP}^{L}$ starts at $\bar{k}_x = \bar{\omega} = 0$ while the lower branch $S_{\rm ISPP}^{U}$ at $\bar{k}_x = 0$, $\bar{\omega} = \bar{\omega}_{\rm IT}$. We find that they are monotonous functions of $\bar{k}_x$. However, at relatively large values of $\bar{k}_x (\gtrsim 2)$, both branches become nearly nondispersive.

We have checked (results are not presented) that as in the structure studied in Fig. 9(b), the single-mode secular equation (26) does not reproduce precisely the exact results obtained employing Eq. (12). A small (depending on $\bar{k}_x$) red-shift of the branches is observed. The black horizontal arrows in Figs. 7 and 8 represent the frequencies of the $S_{\rm ISPP}^{U}$ and $S_{\rm ISPP}^{L}$ branches, at $\bar{k}_x = 2$, obtained employing Eq. (26). We find that, at large $\bar{k}_x$ (i.e., when $\bar{\omega}_S$ is close to $\bar{\omega}_{p,\rm mirr}^{\rm surf} = \bar{\omega}_{\rm IT}$), the red-shifts of both branches are do not differ substantially. It means that then Eq. (26) slightly overestimates the frequencies of the upper and lower branches but reproduces the resonant branch splitting rather well. The origin of the above mentioned red-shift will be discussed at the end of this section.

It is clear from the comparison of Figs. 7 and 8 that the reduction of the mirror separation (or more precisely the reduction of the normalized surface plasmon frequency $\bar{\omega}_{p,\rm mirr}^{\rm surf}$) does not affect the behavior of the branches $S_{\rm ISPP}^{U}$ and $S_{\rm ISPP}^{L}$ dramatically. The situation is different in the case of the branches originating from the antisymmetric mode $A_{\rm SPP}$.

b. Antisymmetric ISPP branches. When, as in the presently discussed structures, $\bar{\omega}_A^{\rm cutoff} \geqslant \bar{\omega}_{p,\rm mirr}^{\rm surf} = \bar{\omega}_{\rm IT}$ then the upper branch $A_{\rm ISPP}^{U}$ starts at $\bar{k}_x = 0$, $\bar{\omega} = \bar{\omega}_A^{\rm cutoff}$ (i.e., in the region $\mathcal{W}_{\rm MQW}^{U}$) as an oscillating-type mode. It changes its character into a surface type after crossing with the $\bar{\alpha}_{\rm MQW}^{U}$ branch at $\bar{k}_x = k_{A_{\rm ISPP}^{U}}^{\rm cross}$. The lower branch $A_{\rm ISPP}^{L}$ also starts as an oscillating-type mode, but at $\bar{k}_x = 0$, $\bar{\omega} = \bar{\omega}_{\rm IT}$ (i.e., in the region $\mathcal{W}_{\rm MQW}^{L}$). Then, it crosses with the $\bar{\alpha}_{\rm MQW}^{L}$ branch at $\bar{k}_x = k_{A_{\rm ISPP}^{L}}^{\rm cross}$ and transforms into a surface-type mode. As one can expect, at large $\bar{k}_x (\gtrsim 2)$ the antisymmetric branch $A_{\rm ISPP}^{U/L}$ practically coincides with the symmetric branch $S_{\rm ISPP}^{U/L}$.

It is worth stressing that the branches $A_{\rm ISPP}^{U}$, $A_{\rm ISPP}^{L}$ and the mode $A_{\rm SPP}$ do not change their character at the same values of $\bar{k}_x$. The results displayed in Figs. 7 and 8 show that $\bar{k}_{A_{\rm ISPP}^{U}}^{\rm cross} < \bar{k}_{A}^{\rm cross} < \bar{k}_{A_{\rm ISPP}^{L}}^{\rm cross}$. It means that the spatial variations of the branches $A_{\rm ISPP}^{U}$ and $A_{\rm ISPP}^{L}$ are not controlled only by the mode function $f_{A,z}$. This fact is not consistent the single-mode cavity approximation. It is reasonable to connect this inconsistency with the presence of the nonresonant coupling of the bright intersubband excitation $P_{1,A}^{\rm MQW}$ with the higher photonic modes (continuum). The above statement seems to be consistent with the fact that, as in the case of the symmetric branches, the exact dispersion curves are slightly red-shifted with respect to the dispersion curves predicted by Eq. (26) based on the single-mode cavity approximation. For illustration of this fact, analogously to the case of the symmetric ISPP branches, we indicate in Figs. 7 and 8 (by the gray horizontal arrows) the frequencies of $A_{\rm ISPP}^{U}$ and $A_{\rm ISPP}^{L}$ branches, at $\bar{k}_x = 2$, obtained employing the single-mode equation (26). Additionally, in Fig. 8 we display (open circles) the dispersion of the branches $A_{\rm ISPP}^{U}$ and $A_{\rm ISPP}^{L}$ predicted by the above-mentioned equation.

In Ref. [18] it has been shown that in the case of the degenerate plasmonic resonators filled with a material possessing (isotropic) excitonic resonances, the formation of the minimum (and consequently the ZGV point) in the A_{SPP} mode implies the formation of the minimum in the upper and lower exciton surface plasmon polariton branches originating from this mode. Moreover, the authors of [18] have demonstrated that such a minimum may serve as a very effective trap for exciton-polariton population at a high nonresonant excitation of the structure. However, in the structures considered in Figs. 7 and 8, we do not observe the formation such a minimum in the A_{ISPP}^U and A_{ISPP}^L branches. Below, we connect this fact with a strong anisotropy of the intersubband excitation.

As mentioned, the above-mentioned anisotropy leads to a strong $\bar{k}_x$ dependence of the overlap factor $F_{A,z}$ (see Fig. 6). Employing Eq. (26), one can check that during the formation of the $A_{ISPP}^{U/L}$ branch, in the degenerate structures, the negative slope of the A_{SPP} mode is dominated by the effects connected with the positive slope of the overlap factor $F_{A,z}$. Consequently, the branches A_{ISPP}^U and A_{ISPP}^L, displayed in Fig. 7, are, in contrast with the A_{SPP} mode, monotonous functions of $\bar{k}_x$. However, as presented in Fig. 5, decreasing $\bar{\omega}_{p,\text{mirr}}$, or more precisely increasing the difference $\bar{\omega}_{p,\text{mirr}}^{\text{crit}} - \bar{\omega}_{p,\text{mirr}}$, we can enhance the dispersion (negative slope at small $\bar{k}_x$) of the A_{SPP} mode. Simulations show that it makes the formation of the minimum in the A_{ISPP}^U branch (at finite $\bar{k}_x$) possible but only for $\bar{\omega}_{p,\text{mirr}}^{\min}$ close to $\omega_{A_{ISPP}^U}^{\min} = 0.431$. (For convenience, we assume that $\bar{\omega}_{p,\text{mirr}}^{\text{surf}} = \bar{\omega}_{IT}$ and $\bar{\varpi}_{p,\text{MQW}} = 0.3 \times \bar{\omega}_{IT}$.) Figure 5(c) illustrates the above-mentioned fact. Unfortunately, the minimum appearing in the A_{ISPP}^U branch is always shallower than the minimum appearing in the A_{SPP} mode supported by the structure with $\bar{\omega}_{p,\text{mirr}}^{\text{surf}} = 0.5$ [see, e.g., Fig. 5(b)]. It means that, unlike the case of the isotropic electronic excitation discussed in Ref. [18], the minimum appearing in the A_{ISPP}^U branch cannot be practically treated as an effective trap for relaxing ISPPs.

Nevertheless, we have checked that in the case of the structures with $\bar{\omega}_{p,\text{mirr}}^{\text{surf}}$ slightly larger than $\omega_{A_{ISPP}^U}^{\min}$ an interesting [particularly in the context of the slow- (stopped-) light effects] situation can be achieved. Namely, assuming that $\bar{\omega}_{p,\text{mirr}}^{\text{surf}} = \bar{\omega}_{IT}$ and taking $\bar{\varpi}_{p,\text{MQW}} = 0.3 \times \bar{\omega}_{IT}$, we have found that the formation of quasidispersionless A_{ISPP}^U branch is possible at $\bar{\omega}_{p,\text{mirr}}^{\text{surf}}$ close to 0.45. (The results are not presented.) As one can expect, for $\bar{\omega}_{p,\text{mirr}}^{\text{surf}}$ substantially smaller than $\bar{\omega}_{A_{ISPP}^U}^{\min}$ (like in Fig. 8) the upper branch A_{ISPP}^U has a negative slope.

It is obvious that additional modification of the A_{ISPP}^U branch is possible by changing the location of the intersubband frequency with respect to the surface plasmon frequency. We do not discuss this case.

c. In-gap ISPP branches. As mentioned, an important consequence of the coupling of the intersubband excitation with the continuum modes is the formation of the (oscillating-type) in-gap polariton branches. They are located slightly below $\bar{\omega}_{IT}$. We have hatched (in Figs. 7, 8, 10, and 11) the frequency range where the in-gap polariton branches appear. We would like to note that, in the nonresonant structures studied in Fig. 9, such branches are also present but we did not plot them in order to concentrate on the behavior of the S_{ISPP}^U and S_{ISPP}^L branches.
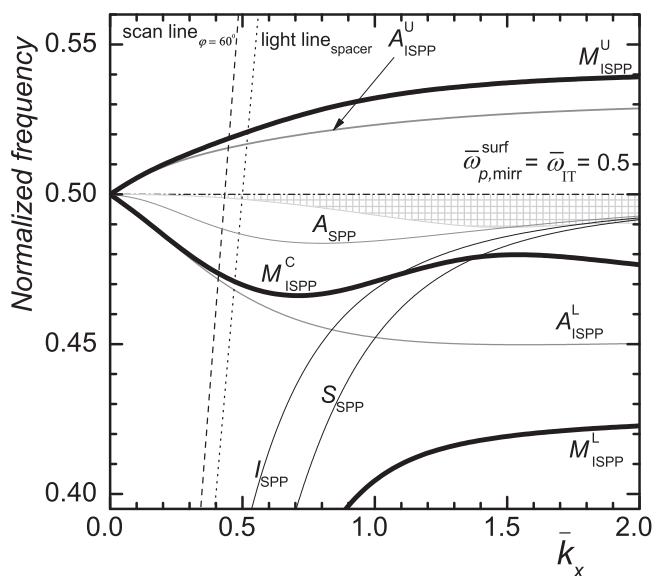

FIG. 10. The normalized frequencies of the hybrid ISPP branches supported by the four-layer structure as a function of $\bar{k}_x$ (the thick solid curves). For illustration, the normalized frequency of the modes A_{SPP} and S_{SPP}, as well as the normalized frequencies of the branches A_{ISPP}^U and A_{ISPP}^L supported by the three-layer structure with $\bar{\varpi}_{p,\text{MQW}} = 0.3 \times \bar{\omega}_{IT}$ are also displayed (the thin solid curves). The short-dotted (dashed-dotted) line corresponds to the spacer light line (the normalized intersubband frequency $\bar{\omega}_{IT}$ and surface plasma frequency $\bar{\omega}_{p,\text{mirr}}^{\text{surf}}$). The interpretation of the scan line (dashed line) is given in Appendix D. The hatched area indicates the $\bar{\omega}$ region where the in-gap polariton branches are located. $\bar{\omega}_{p,\text{mirr}}^{\text{surf}} = \bar{\omega}_{IT} = 0.5$ and $\bar{\varpi}_{p,\text{MQW}} = \sqrt{2} \times (0.3 \times \bar{\omega}_{IT})$.

Inspection of the results presented in Figs. 7 and 8 indicates that the role of coupling with higher photonic modes increases with increasing $\bar{k}_x$. However, we should remember that accuracy of the semiclassical approach and the quasiparticle approach employed in this paper seems to be
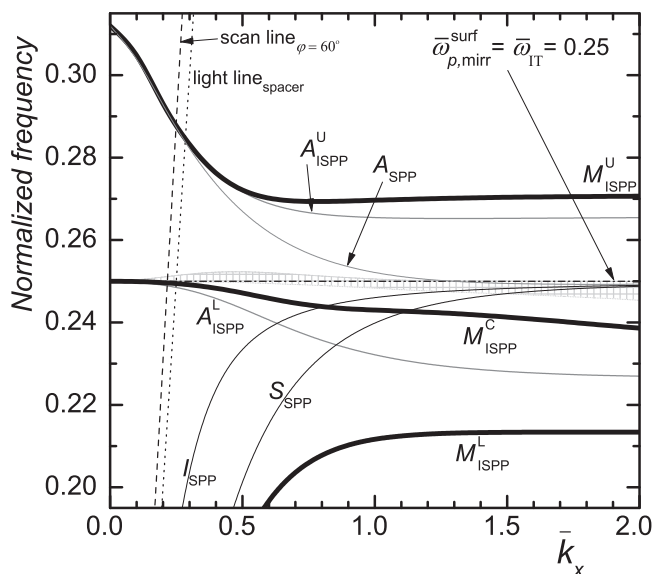

FIG. 11. Same as in Fig. 10, except that now $\bar{\omega}_{p,\text{mirr}} = \bar{\omega}_{IT} = 0.25$.

insufficient for correct description of the polariton branches in the limit of large value of $\bar{k}_x$. It is connected with the fact that the above-mentioned approaches are based on the long-wavelength approximation. This approximation breaks down when electromagnetic modes interacting with intersubband excitation varies substantially in the region of the QW [73].

B. Four-layer structures

Now, we discuss the properties of the ISPP branches originating from the plasmonic modes in four-layer asymmetric structures. In such structures, only half of the space between mirrors is occupied by an MQW slab. The second half of the space is occupied by a dielectric spacer layer with a dielectric constant $\varepsilon_{spac} = \varepsilon_w$ [see Fig. 1(b)].

The numerical solutions of the frequency dispersion equation (11) for such type structures are displayed in Figs. 10 and 11. As in the previous subsection, we discuss the degenerate structure ($\bar{\omega}_{p,\text{mirr}}^{\text{surf}} = \bar{\omega}_{\text{IT}} = 0.5$) and the nearly degenerate structure ($\bar{\omega}_{p,\text{mirr}}^{\text{surf}} = \bar{\omega}_{\text{IT}} = 0.25$). As mentioned at the beginning of this section, for the convenience of comparison with three-layer structures discussed in Figs. 7 and 8, we take $\bar{\omega}_{p,\text{MQW}} = \sqrt{2} \times (0.3 \times \bar{\omega}_{\text{IT}})$.

The inspection of Figs. 10 and 11 shows that now, unlike in the case of symmetric structures, the ISPP branches originating from the plasmonic modes do not form two independent pairs of (symmetric and antisymmetric) branches. Instead, we observe the formation of three (multimode) branches denoted as the upper branch (M_{ISPP}^U), the central branch (M_{ISPP}^C), and the lower branch (M_{ISPP}^L). In both systems, the branches M_{ISPP}^U and M_{ISPP}^L are monotonous functions of $\bar{k}_x$. For larger values of $\bar{k}_x$ ($\gtrsim 2$), they are practically nondispersive. For small values of $\bar{k}_x$ ($\lesssim 0.5$), the branches M_{ISPP}^U and M_{ISPP}^L practically coincide with the branches A_{ISPP}^U and A_{ISPP}^L originating from the antisymmetric mode of the three-layer structures characterized by two times smaller values $\bar{\omega}_{p,\text{MQW}}^2$.

The behavior of the central branch M_{ISPP}^C is more complex (particularly in the degenerate structure discussed in Fig. 10) than that of branches M_{ISPP}^U and M_{ISPP}^L. For example, we observe that in the degenerate structure, the central branch M_{ISPP}^C is strongly nonmonotonous. More specifically, we observe the formation of the two ZGV points at $\bar{k}_x \cong 0.7$ and $\bar{k}_x \cong 1.55$.

In our opinion, the results displayed in Figs. 10 and 11 are consistent with our previous statement (see Sec. III) that the main features of the branches M_{ISPP}^U, M_{ISPP}^L, and M_{ISPP}^C supported by the four-layer structures are rather well captured by the three-oscillator model described by Eq. (35). For example, the anticrossing behavior of the S_{SPP} mode and the A_{ISPP}^L branch, predicted by the three-oscillator model, is well pronounced in the degenerate structure (see Fig. 10) at $\bar{k}_x \approx 1$. We find also that, in agreement with the three-oscillator model, half of the asymptotic separation between the branches M_{ISPP}^U and M_{ISPP}^L is larger than the asymptotic coupling frequency (corresponding to the modes S_{SPP} and A_{SPP}) by factor close to $\sqrt{2}$. Nevertheless, some inconsistencies with the three-oscillator model, particularly in the behavior of the central mode, are observed. The reason for these inconsistencies is briefly discussed below.

It is obvious that, as in the case of the symmetric structures, also in the asymmetric structures the formation of the in-gap

polariton branches takes place. (We have hatched, in Figs. 10 and 11, areas where they are positioned.) The formation of such branches is not included in the three-oscillator model. The detailed inspection of the presented results suggests that, particularly in the case of the degenerate structure studied in Fig. 10, we can speak about a resonant interaction (or equivalently the anticrossing) of the M_{ISPP}^C branch with the in-gap branches. This anticrossing is observed at $\bar{k}_x \approx 1.5$. As mentioned, its appearance can be associated with the presence of the "nondiagonal" coupling.

The characteristics of the polariton branches presented and discussed in this paper have been obtained neglecting the dissipation. In Appendix D we validated this approximation, demonstrating that the lossless branches manifest in the reflection-absorption spectra of the realistic structures based on GaAsAl.

VII. CONCLUSIONS

The dispersion characteristics of the intersubband surface plasmon polaritons (ISPPs) supported by all-semiconductor three- and four-layer planar plasmonic resonators have been investigated theoretically. Manifestation of the above-mentioned polariton branches in reflection-absorption spectra of the realistic structures is additionally discussed. A semiclassical approach based on the transfer matrix formalism and the effective-medium approximation has been employed.

The results obtained indicate that the behavior of the ISPP branches can be in large extent modified changing the normalized mirror plasma frequency $\bar{\omega}_{p,\text{mirr}}$. However, the character of the modification is strongly affected by the asymmetry of the structures and anisotropy of the intersubband excitation. We have shown that, particularly in the case of asymmetric structures, the dispersion characteristics of the ISPP branches can be engineered in the context of the slow- and stopped-light phenomena, i.e., formation of the ZGV points.

Simulations reveal that the correct quasiparticle interpretation of the dispersion characteristics is possible employing the concept of the bright and dark intersubband excitations. However, calculating the mode overlap factors we should take into account the dispersive character of the plasmonic mirrors and anisotropy of the intersubband excitation. We show also that the effects resulting from the coupling of the bright and dark intersubband excitations with higher resonator modes play a non-negligible role, particularly at large $\bar{k}_x$. Interpretation of the results obtained for the asymmetric structures is additionally complicated by the formation of the multimode ISPP branches. They are responsible for the appearance of the effect similar to the "polariton-induced optical asymmetry" observed in the absorption spectra of the coupled semiconductor microcavity structures containing QW in one of the cavities [42,43,46].

It seems that it would be interesting to investigate the dispersion characteristics of the ISPP branches supported by resonators with different claddings or more precisely with different plasmon frequencies. As shown in Refs. [75,76], the differentiation of the plasma frequencies of the cladding leads to substantial modification of the plasmonic mode behavior. It adds another important degree of freedom in manipulation of the ISPP branches.

It is also reasonable to expect that, due to extraordinary properties of the carriers in graphene (in particular the electrical tunability of the carrier density), very interesting physics should appear in the case of the resonators where not uniformly doped semiconductor layers but graphene-based [77–79] (or all-semiconductor-based [52]) hyperbolic metamaterials play a role of the plasmonic mirrors.

Finally, we would like to stress that in this paper we have restricted to the linear intersubband response. Results reported in Ref. [46] for the coupled microcavities suggest that the nonlinear intersubband response of the plasmonic resonators should be more complex than standard semiconductor resonators discussed in our previous paper [80]. The case of the nonlinear (saturated) intersubband response of the three- and four-layer structures is planned to be presented in a later paper.

APPENDIX A: RESONATORS WITH NONEQUISPACED QWS

The expression for the coupling frequency $\Omega_{R,\mathcal{N}}$ presented in Sec. IV B has been derived assuming that the MQW slab contains a large number ($N_{\mathrm{QW}} \gg 1$) of equispaced QWs. Below, we present the expression for the coupling frequency when QWs are arbitrarily positioned inside the plasmonic resonator.

In the simplest case when a single QW couples with the TEM mode, the (electric dipole gauge) coupling frequency can be written as [5,37]

$$\check{\Omega}_{R,\mathrm{TEM}}^2 = \frac{f_{\mathrm{IT}} N_s e^2}{4 m_w^* \varepsilon_0 \varepsilon_w L_{\mathrm{MC}}}. \tag{A1}$$

Now, let us assume that the QWs, positioned at $z = z_\iota, \ldots, z_{N_{\mathrm{QW}}}$, couple resonantly to the $\mathcal{N}$th plasmonic mode ($n_{\mathrm{res}} \equiv \mathcal{N}$). At this point, it is convenient to employ the concept of the spatial dependent of the effective mode length introduced in the literature for the systems with dielectric (see, e.g., [5,56,59]) and plasmonic (see, e.g., [58,60,63]) mirrors. Then, we get the following generalized expression for the coupling frequency between the $\mathcal{N}$th plasmonic mode and the bright excitation of the nonequispaced QWs:

$$\Omega_{R,\mathcal{N}}^2 = \check{\Omega}_{R,\mathrm{TEM}}^2 L_{\mathrm{MC}} / \mathcal{L}_{\mathcal{N}}^{\mathrm{eff}}, \tag{A2}$$

where $\mathcal{L}_{\mathcal{N}}^{\mathrm{eff}} = \sum_{\iota=1}^{N_{\mathrm{QW}}} L_{\mathcal{N},z}^{\mathrm{eff}}(z_\iota)$. The quantity

$$L_{N,z}^{\mathrm{eff}}(z) = U_N^{\mathrm{total}} / \varepsilon_0 \varepsilon_w |E_{N,z}(z)|^2 \tag{A3}$$

can be treated as the z-dependent effective length of the Nth mode ($N = S, A, I$). The explicit expression for the dimensionless parameter $\underline{L}_{N,z}^{\mathrm{eff}} = L_{N,z}^{\mathrm{eff}} / L_{\mathrm{MC}}$ is given in Appendix C.

The $\bar{k}_x$ dependence of $1/\underline{L}_{N,z}^{\mathrm{eff}}$ calculated for the different value of the (normalized) QW mirror distance $\underline{z}_{\mathrm{QW}} = (L_{\mathrm{MC}}/2 - z)/L_{\mathrm{MC}}$ presents Fig. 12. A different behavior of $\underline{L}_{S,z}^{\mathrm{eff}}(\bar{k}_x, \underline{z}_{\mathrm{QW}})$ and $\underline{L}_{A,z}^{\mathrm{eff}}(\bar{k}_x, \underline{z}_{\mathrm{QW}})$ is connected mainly with different spatial variation of the squared mode functions $|f_{S,z}|^2$ and $|f_{A,z}|^2$. At large value of $\bar{k}_x$ ($\gtrsim 2$), the difference between the above-mentioned functions practically vanishes. It implies that the difference between $\underline{L}_{S,z}^{\mathrm{eff}}(\bar{k}_x, \underline{z}_{\mathrm{QW}})$ and $\underline{L}_{A,z}^{\mathrm{eff}}(\bar{k}_x, \underline{z}_{\mathrm{QW}})$ also vanishes.

It is worth noting that at large $\bar{k}_x$ the ratio $\underline{L}_{N,z}^{\mathrm{eff}}(\bar{k}_x, \underline{z}_{\mathrm{QW}}) / \underline{L}_{I,z}^{\mathrm{eff}}(\bar{k}_x, \underline{z}_{\mathrm{QW}})$ is close to 2 not 1. The appearance of
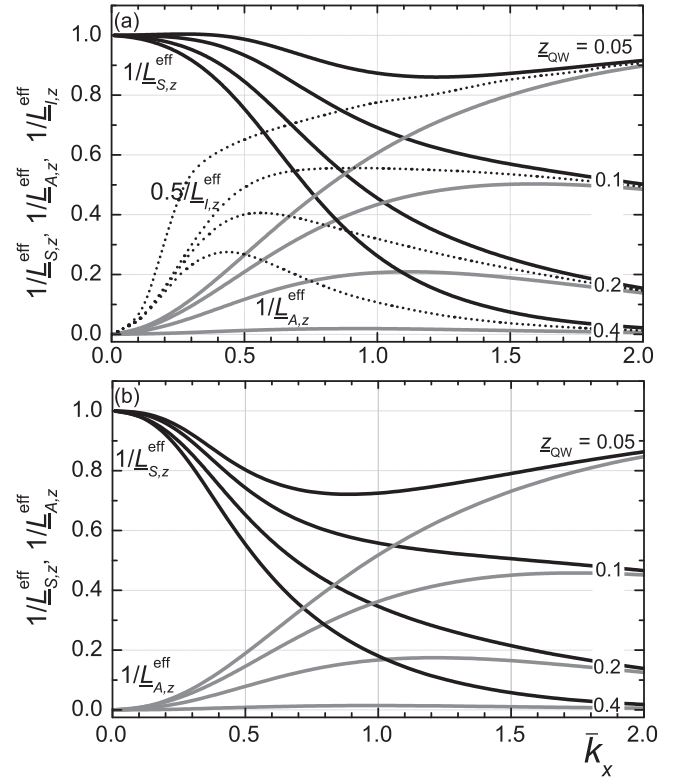

FIG. 12. The $\bar{k}_x$ dependence of reciprocal of the normalized effective mode length corresponding to the modes S_{SPP} (black solid curves), A_{SPP} (gray solid curves), and I_{SPP} (dotted curves) calculated for different values of the normalized distance $\underline{z}_{\mathrm{QW}} = (L_{\mathrm{MC}}/2 - z)/L_{\mathrm{MC}}$. (a) The structure with $\bar{\omega}_{p,\mathrm{mirr}}^{\mathrm{surf}} = 0.5$ and (b) the structure with $\bar{\omega}_{p,\mathrm{mirr}}^{\mathrm{surf}} = 0.25$.

the factor 2 results from the fact that at large $\bar{k}_x$, the plasmonic modes $S_{\mathrm{SPP}}/A_{\mathrm{SPP}}$ can be considered as a symmetric/antisymmetric combination of the two single-interface modes I_{SPP}. Consequently, the spatial extent of the electromagnetic confinement of the single-interface mode I_{SPP} is then nearly two times smaller than the modes S_{SPP} and A_{SPP}.

It is obvious that the effective-medium approximation is not appropriate for the systems with nonequispaced QWs. Then, the components of the transfer matrix describing the system can be calculated numerically modeling the quasi-two-dimensional electron gas, in each QW, by 2D sheet positioned at the center of the QW [47,80].

APPENDIX B: DETAILS ON THE EIGENMODE SOLUTIONS

Substituting relations (5) and (6) into the Maxwell's curl equation, we arrive at the following set of coupled equations for components E_x, E_z, and H_y in the (passive) resonator [11]:

$$i\omega \mu_0 H_y = dE_x/dz - ik_x E_z, \tag{B1}$$

$$i\omega \varepsilon_0 \varepsilon E_x = dH_y/dz, \tag{B2}$$

$$i\omega \varepsilon_0 \varepsilon E_z = -ik_x H_y, \tag{B3}$$

where

$$\varepsilon(z,\omega) = \begin{cases} \varepsilon_w & \text{for } |z| < L_{\text{MC}}/2, \\ \varepsilon_{\text{mirr}}(\omega) & \text{for } |z| > L_{\text{MC}}/2 \end{cases} \quad (B4)$$

is the z-dependent dielectric function of the passive resonator.

Using (B2) and (B3), we get an additional relation

$$E_x = (i/k_x)dE_z/dz. \quad (B5)$$

Thus, the components E_x and H_y can be written in the terms of E_z. (As already mentioned, only the z component of the displacement field $D_z = \varepsilon_0 \varepsilon E_z$ couples with the intersubband excitation.) From Eqs. (B1)–(B5) one finds that the E_z satisfies the Helmholtz equation

$$d^2 E_z/dz^2 + (\varepsilon K^2 - k_x^2)E_z = 0. \quad (B6)$$

According to the boundary conditions for the EM field, D_z and E_x must be continuous at mirror surfaces. Moreover (in the case of bound modes), E_z must vanish for $z \to \pm\infty$. It leads to the eigenmode equation (41).

Due to the symmetry of the considered structure, the z and x components of the electric field $\mathbf{E}_{\mathcal{N}}$ associated with $\mathcal{N}$th mode obey the following relations: $E_{S,z}(z) = E_{S,z}(-z)$, $E_{A,z}(z) = -E_{A,z}(-z)$ and $E_{S,x}(z) = -E_{S,x}(-z)$, $E_{A,x}(z) = E_{A,x}(-z)$. Thus, the spatial variation of the above-mentioned components can be considered only for $z > 0$.

In $z > L_{\text{MC}}/2$,

$$E_{\mathcal{N},z}(z) = \mathcal{A}_{\mathcal{N}} \mathcal{B}_{\mathcal{N}} \exp(-\alpha_{\text{mirr},\mathcal{N}} z), \quad (B7)$$

$$E_{\mathcal{N},x}(z) = \mathcal{A}_{\mathcal{N}} \mathcal{B}_{\mathcal{N}}(-i\alpha_{\text{mirr},\mathcal{N}}/k_x)\exp(-\alpha_{\text{mirr},\mathcal{N}} z), \quad (B8)$$

and in $0 < z < L_{\text{MC}}/2$,

$$E_{S,z}(z) = \mathcal{A}_S \cosh(\alpha_{\text{spac},S} z), \quad (B9)$$

$$E_{S,x}(z) = \mathcal{A}_S(i\alpha_{\text{spac},S}/k_x)\sinh(\alpha_{\text{spac},S} z), \quad (B10)$$

$$E_{A,z}(z) = \mathcal{A}_A \sinh(\alpha_{\text{spac},A} z), \quad (B11)$$

$$E_{A,x}(z) = \mathcal{A}_A(i\alpha_{\text{spac},A}/k_x)\cosh(\alpha_{\text{spac},A} z). \quad (B12)$$

Here, $\mathcal{A}_S$ and $\mathcal{A}_A$ are arbitrary constants with units of electric field that are used to normalize the modes. Moreover,

$$\mathcal{B}_{\mathcal{N}} = \exp(\alpha_{\text{mirr},\mathcal{N}} L_{\text{MC}}/2)(\varepsilon_w/\varepsilon_{\text{mirr},\mathcal{N}})$$
$$\times \begin{cases} \cosh(\alpha_{\text{spac},S} L_{\text{MC}}/2) & \text{for } \mathcal{N} = S, \\ \sinh(\alpha_{\text{spac},A} L_{\text{MC}}/2) & \text{for } \mathcal{N} = A, \end{cases} \quad (B13)$$

where $\alpha_{\text{spac/mirr},\mathcal{N}} = \alpha_{\text{spac/mirr}}(\bar\omega = \bar\omega_{\mathcal{N}})$. The above equations give information on the spatial variation of the plasmonic mode functions $f_{S,z}$ and $f_{A,z}$ appearing in Eq. (21).

In the idealized case when cladding material can be treated as a perfect metal ($\varepsilon_{\text{mirr}} \to -\infty$), the nth-cavity-mode function simplifies to the form

$$f_{n,z}^{\text{perf}}(z) = \begin{cases} \cos(n\pi z/L_{\text{MC}}) & \text{for } n = 0,2,4\ldots, \\ \sin(n\pi z/L_{\text{MC}}) & \text{for } n = 1,3,5\ldots. \end{cases} \quad (B14)$$

The (normalized) mode frequency is then given by

$$\bar\omega_n^{\text{perf}} = (\bar k_x^2 + n^2)^{1/2}. \quad (B15)$$

APPENDIX C: EXPRESSIONS FOR OVERLAP FACTOR AND EFFECTIVE MODE LENGTH

Substituting Eqs. (B7)–(B13) into Eq. (33) and performing the integrations we find that the expression for the overlap factor $F_{\mathcal{N},z}$ can be written in the following form:

$$F_{\mathcal{N},z} = u_{\mathcal{N},z}^{\text{spac}}/u_{\mathcal{N}}^{\text{total}}. \quad (C1)$$

Here, $u_{\mathcal{N}}^{\text{total}} = u_{\mathcal{N},x}^{\text{spac}} + u_{\mathcal{N},z}^{\text{spac}} + u_{\mathcal{N}}^{\text{mirr}}$ where

$$u_{\mathcal{N}}^{\text{mirr}} = 2\int_{L_{\text{MC}}/2}^{\infty} |\mathbf{E}_{\mathcal{N}}|^2 dz$$
$$= |\mathcal{A}_{\mathcal{N}}|^2 L_{\text{MC}}|\mathcal{B}_{\mathcal{N}}|^2 \left(1 + \frac{\bar\alpha_{\text{mirr},\mathcal{N}}^2}{\bar k_x^2}\right) \frac{\exp(-\bar\alpha_{\text{mirr},\mathcal{N}}\pi)}{\bar\alpha_{\text{mirr},\mathcal{N}}\pi}, \quad (C2)$$

$$u_{S,x}^{\text{spac}} = 2\int_0^{L_{\text{MC}}/2} |E_{S,x}|^2 dz$$
$$= |\mathcal{A}_{\mathcal{N}}|^2 \frac{L_{\text{MC}}}{2} \frac{\bar\alpha_{\text{spac},S}^2}{\bar k_x^2}\left[\frac{\sinh(\bar\alpha_{\text{spac},S}\pi)}{\bar\alpha_{\text{spac},S}\pi} - 1\right], \quad (C3)$$

$$u_{S,z}^{\text{spac}} = 2\int_0^{L_{\text{MC}}/2} |E_{S,z}|^2 dz$$
$$= |\mathcal{A}_{\mathcal{N}}|^2 \frac{L_{\text{MC}}}{2}\left[\frac{\sinh(\bar\alpha_{\text{spac},S}\pi)}{\bar\alpha_{\text{spac},S}\pi} + 1\right], \quad (C4)$$

$$u_{A,x}^{\text{spac}} = \int_0^{L_{\text{MC}}/2} |E_{A,x}|^2 dz$$
$$= |\mathcal{A}_{\mathcal{N}}|^2 \frac{L_{\text{MC}}}{2} \frac{|\bar\alpha_{\text{spac},A}|^2}{\bar k_x^2}\begin{cases} \frac{\sin(|\bar\alpha_{\text{spac},A}|\pi)}{|\bar\alpha_{\text{spac},A}|\pi} + 1, & \text{if } \bar k_x < \bar k_A^{\text{cross}} \\ \frac{\sinh(\bar\alpha_{\text{spac},A}\pi)}{\bar\alpha_{\text{spac},A}\pi} + 1, & \text{if } \bar k_x > \bar k_A^{\text{cross}} \end{cases} \quad (C5)$$

$$u_{A,z}^{\text{spac}} = 2\int_0^{L_{\text{MC}}/2} |E_{A,z}|^2 dz$$
$$= |\mathcal{A}_{\mathcal{N}}|^2 \frac{L_{\text{MC}}}{2}\begin{cases} 1 - \frac{\sin(|\bar\alpha_{\text{spac},A}|\pi)}{|\bar\alpha_{\text{spac},A}|\pi}, & \text{if } \bar k_x < \bar k_A^{\text{cross}} \\ \frac{\sinh(\bar\alpha_{\text{spac},A}\pi)}{\bar\alpha_{\text{spac},A}\pi} - 1, & \text{if } \bar k_x > \bar k_A^{\text{cross}}. \end{cases} \quad (C6)$$

Finally, we would like to stress that when, as in Refs. [18,72], the electronic excitation is isotropic, then $F_{\mathcal{N},z}$ given by Eq. (C1) should be replaced by $F_{\mathcal{N}} = (u_{\mathcal{N},x}^{\text{spac}} + u_{\mathcal{N},z}^{\text{spac}})/u_{\mathcal{N}}^{\text{total}}$. Such a substitution affects particularly strongly the $\bar k_x$ dependence of the overlap factor corresponding to the antisymmetric mode. More precisely, in the case of the isotropic electronic excitation the overlap factors corresponding to the plasmonic modes are much flatter than that displayed in Fig. 6 (results are not presented). It explains why in the case of the isotropic excitations studied in Ref. [18], the antisymmetric exciton surface plasmon polariton branches are nearly parallel (in the ω-k_x plane) to the A_{SPP} mode.

For completeness, we have also calculated the (normalized) spatial-dependent effective mode length $\underline{L}_{N,z}^{\text{eff}} = L_{N,z}^{\text{eff}}/L_{\text{MC}}$, where $L_{N,z}^{\text{eff}}$ is defined in Appendix A. Performing appropriate

manipulations, we get the following result:

$$\underline{L}_{\mathcal{N},z}^{\text{eff}}(\bar{z}) = \frac{\mathrm{u}_{\mathcal{N}}^{\text{total}}}{L_{\text{MC}}|\mathcal{A}_{\mathcal{N}}|^2} \times \begin{cases} |\cosh(\bar{\alpha}_{\text{spac},S}\bar{z})|^{-2} & \text{for } \mathcal{N} = S, \\ |\sinh(\bar{\alpha}_{\text{spac},A}\bar{z})|^{-2} & \text{for } \mathcal{N} = A, \end{cases}$$

(C7)

$$\underline{L}_{I,z}^{\text{eff}}(\underline{z}_{\text{QW}}) = \frac{\exp(2\bar{\alpha}_{\text{spac},I}\pi \underline{z}_{\text{QW}})}{2\bar{\alpha}_{\text{mirr},I}\pi}\left[1 + \frac{\bar{\alpha}_{\text{spac},I}^2}{\bar{k}_x^2}\right. \\ \left. + \left(1 + \frac{\bar{\alpha}_{\text{mirr},I}^2}{\bar{k}_x^2}\right)\left(\frac{\varepsilon_w}{\varepsilon_{\text{mirr},I}}\right)^2\right],$$

(C8)

where $\varepsilon_{\text{mirr},I} = \varepsilon_{\text{mirr}}(\bar{\omega} = \bar{\omega}_I)$ and $\underline{z}_{\text{QW}} = (L_{\text{MC}}/2 - z)/L_{\text{MC}}$. One can check that the formula (C8) gives the numerical results equivalent to those predicted by Eq. (33) in Ref. [65] provided that the factor π^2 appearing in this equation is removed.

APPENDIX D: REFLECTION-ABSORPTION SPECTRA AND POLARITON-INDUCED OPTICAL ASYMMETRY

Now, we discuss the optical response of the three- and four-layer structures assuming that one of the mirrors (the coupling mirror) has a finite thickness d_{mirr}. Through this mirror, external radiation couples to the electromagnetic modes supported by the structure. It is well known that when the open resonator operates in the strong coupling regime, the peak positions in the angle-resolved absorption spectra are close to the frequency of the electromagnetic modes supported by the idealized nondissipative structures with totally reflecting mirrors [38]. Below, we illustrate the above statement performing numerical calculations for realistic systems.

1. Description of the GaAs/GaAsAl-based open resonators

As mentioned, we consider systems based on GaAs/GaAsAl. For simplicity, the difference between $\varepsilon_{\text{GaAs}}(=\varepsilon_w)$ and $\varepsilon_{\text{GaAsAl}}$ is omitted. We assume also that the coupling mirror, with thickness $d_{\text{mirr}} > \alpha_{\text{mirr},\mathcal{N}}^{-1}$, is backed by the semi-infinite medium with dielectric constant $\varepsilon_{\text{back}} = \varepsilon_w$. Moreover, in the case of the four-layer structures, we discuss two configurations, namely, when the MQW slab is located near the coupling mirror (the structure type C) and near the back mirror (the structure type B).

The dielectric function of the mirrors is described by a Drude model with a realistic value of damping rate $\gamma_{\text{mirr}}(= 10 \text{ meV}/\hbar)$. As in Ref. [10] we take $N_D = 5 \times 10^{18} \text{ cm}^{-3}$. It corresponds to $\hbar\omega_{p,\text{mirr}}^{\text{surf}} = 69.3 \text{ meV}$ [see Eq. (4)]. The rest of the parameters have been taken consistent with structures studied in Figs. 7, 8, 10, and 11. Additionally, to facilitate the comparison of the results obtained for the symmetric and asymmetric structures, we have assumed (as in Sec. VI) that the number of the QWs, the product $f_{\text{IT}}N_S$, and intersubband frequency are the same in all the structures: $N_{\text{QW}} = 26$, $f_{\text{IT}}N_S = 1.15 \times 10^{12} \text{ cm}^{-2}$, and $\omega_{\text{IT}} = \omega_{p,\text{mirr}}^{\text{surf}} = 69.3 \text{ meV}$. In the case of the thicker (thinner) structure, we take $L_{\text{MC}} = 13.468 \, \mu\text{m}$ (6.734 μm) what corresponds to $\bar{\omega}_{p,\text{mirr}}^{\text{surf}} = 0.5 \, (0.25)$. As mentioned at the beginning of Sec. VI, the period (d_{MQW}) of the MQW slab, located in the four-layer structure, is two times smaller than the period of the MQW slab located in the three-layer structure. It implies that in the case of the
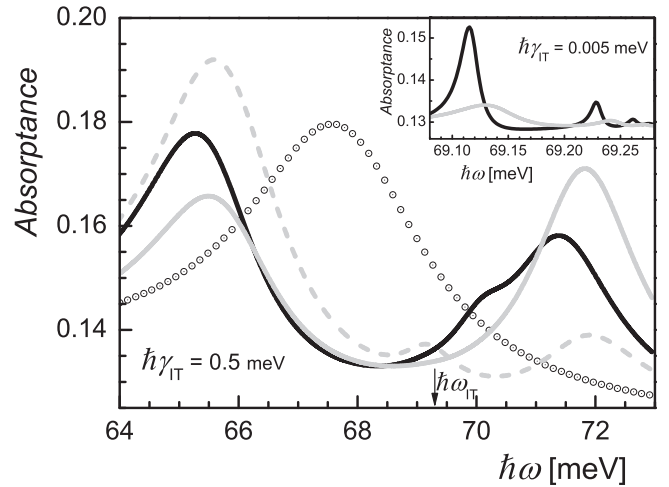

FIG. 13. The spectral dependence of the absorptance of the passive structure (open circles), the three-layer (black solid curves) and four-layer (gray solid and dashed curves) structures described in the text. The gray dashed (solid) curve corresponds to the four-layer structure with the MQW located near the coupling (back) mirror. The calculations have been performed taking $\hbar\gamma_{\text{IT}} = 0.5 \text{ meV}$ and $\hbar\gamma_{\text{IT}} = 0.005 \text{ meV}$ (see the inset). $\omega_{p,\text{mirr}}^{\text{surf}} = \omega_{\text{IT}} = 69.3 \text{ meV}$ and $L_{\text{MC}} = 13.468 \, \mu\text{m}$. It corresponds to $\bar{\omega}_{p,\text{mirr}}^{\text{surf}} = \bar{\omega}_{\text{IT}} = 0.5$.

three- (four-) layer structure, the relation $\varpi_{p,\text{MQW}} = 0.3 \times \omega_{\text{IT}}$ $[\varpi_{p,\text{MQW}} = \sqrt{2} \times (0.3 \times \omega_{\text{IT}})]$ is valid. Thus, the coupling frequencies in the symmetric and asymmetric structures coincide. For the convenience of presentation, the intersubband damping rate γ_{IT} will be treated as a free parameter.

Numerical calculations have been performed assuming that light incidents from the backed medium at the angle $\varphi_{\text{inc}} = 60°$ on the coupling mirror with thickness $d_{\text{mirr}} = 20 \, \mu\text{m}$. We have checked that a further increase of the mirror thickness practically does not affect the position of the peak in the absorption-reflection spectra. The above-mentioned peaks should be located near the crossings of the scan line $\bar{k}_x = \bar{K}\varepsilon_w^{1/2}\sin\varphi_{\text{inc}}$ (represented in Figs. 10 and 11 by a thin dashed line) with appropriate polariton branches [37,38].

2. Manifestation of the ISPP branches in absorption spectra and polariton-induced optical asymmetry

The inspection of the numerical results displayed in Figs. 13 and 14 leads to the conclusions consistent with the theoretical results reported in Ref. [34]. Namely, taking sufficiently small values of parameter $\gamma_{\text{IT}} = 0.5 \text{ meV}$ we are able to resolve all the peaks associated with the ISPP branches discussed in Sec. VI. For example, in the case of the degenerate four-layer structure discussed in Fig. 13, the peak in the solid gray curve appearing at $\hbar\omega \cong 65.5 \text{ meV}$ ($\hbar\omega \cong 72 \text{ meV}$) can be associated with the M_{ISPP}^C (M_{ISPP}^U) branch represented by appropriate thick curves in Fig. 10. The above-mentioned peaks are resolved even when we take a more realistic value of the parameter γ_{IT}, e.g., $\gamma_{\text{IT}} = 5 \text{ meV}$. (Results are not presented.) Nevertheless, we would like to stress that the relative branch splittings extracted from Figs. 13 and 14 are slightly smaller than those predicted by Figs. 5, 7, 8, 10, and 11. This difference is due to the fact that solving dispersion equations (11) and
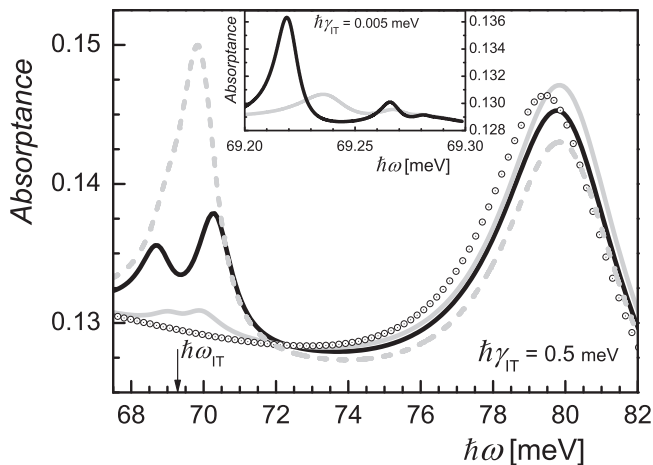
FIG. 14. Same as in Fig. 12, except that now $L_{MC} = 6.734 \ \mu$m. It corresponds to $\bar{\omega}_{p,\mathrm{mirr}}^{\mathrm{surf}} = \bar{\omega}_{\mathrm{IT}} = 0.25$.

(12) we have completely neglected dissipative losses. We also find that the higher-order in-gap branches (see the insets in Figs. 13 and 14) can be resolved only partially taking unrealistically small values of γ_{IT} ($\lesssim 10^{-4} \times \omega_{\mathrm{IT}}$). It means that the observation of the in-gap branches in the reflection/absorption spectra of realistic structures seems to be extremely difficult.

The inspection of Figs. 13 and 14 also shows that in the case of the asymmetric structures, the reflection/absorption spectrum is sensitive to the location of the MQW slab with respect to the coupling mirror. In other words, the spectra of the C and B type structures differ substantially. A similar effect has been observed by Armitage *et al.* [42] (see also [43]) in the coupled semiconductor microcavity structures containing QW in one of the cavities. (The authors named this effect "polariton-induced optical asymmetry.") At this point, it worth noting that the above-mentioned difference in the reflection-absorption spectra of the C and B type asymmetric structures is consistent with the general constraint. This constraint predicts the light reflection nonreciprocity for two-side incidence when the dissipation and asymmetry are simultaneously present in the structure [81]. Below, we present a semiqualitative description of the above-mentioned asymmetry in the absorption spectra of the C and B type four-layer structures.

Let us assume that (for given value of $\bar{k}_x$) the coupling of the two single-interface (I_{SPP}) plasmonic modes, leading to the formation the S_{SPP} and A_{SPP} modes, is relatively weak. From Eq. (40), one finds that it is equivalent to the assumption that $|\omega_{\mathcal{N}} - \omega_I| \ll \omega_I$. In the considered systems (see Figs. 2 and 3), the above condition is fulfilled when $\bar{k}_x$ is sufficiently large ($\gtrsim 0.5$). Then, assuming additionally that the RWA is valid, it is convenient to model the four-layer structure discussed in Figs. 13 and 14 with the help of the (modified) three-coupled-oscillator model similar to that developed in Ref. [42]. The main difference from the three-coupled-oscillator model

discussed in Sec. IV C is the following. Now, the two plasmonic oscillators are connected, not with the modes S_{SPP} and A_{SPP}, but with the single-interface surface plasmon modes $I_{\mathrm{SPP}}^{\mathsf{C}}$ and $I_{\mathrm{SPP}}^{\mathsf{B}}$, localized at the coupling and back mirrors, respectively. Moreover, the intersubband oscillator is connected with the bright intersubband excitation having the same spatial variation as the $I_{\mathrm{SPP}}^{\mathsf{C}}$ ($I_{\mathrm{SPP}}^{\mathsf{B}}$) mode when the MQW slab is located at the coupling (back) mirror. It is reasonable to assume that, in the case of the C (B) type structure, the intersubband oscillator couples practically only to the $I_{\mathrm{SPP}}^{\mathsf{C}}$ ($I_{\mathrm{SPP}}^{\mathsf{B}}$) plasmonic oscillator. As already mentioned, the coupling between plasmonic oscillators, i.e., between the modes $I_{\mathrm{SPP}}^{\mathsf{C}}$ and $I_{\mathrm{SPP}}^{\mathsf{B}}$, is controlled by the coupling factor κ_I. Such a modified three-coupled-oscillator model leads to the effective Hamiltonian having the same form as that given by Eq. (1) in Ref. [42]. Such a type Hamiltonian predicts the formation of the three (multimode) branches denoted, for convenience, by $\mathsf{M}_{\mathrm{ISPP}}^{U}$ (upper branch), $\mathsf{M}_{\mathrm{ISPP}}^{C}$ (central branch), and $\mathsf{M}_{\mathrm{ISPP}}^{L}$ (lower branch). These branches practically coincide with the branches predicted by the Hamiltonian (35) discussed in Sec. IV C, provided that the mentioned above condition $|\omega_I - \omega_{\mathcal{N}}| \ll \omega_I$ is fulfilled and the structure is nearly degenerate.

Employing the modified three-coupled-oscillator mode, one finds (for details see [42]) that, in the particular case when $\omega_I = \omega_{\mathrm{IT}}$, the eigenvector of the branch $\mathsf{M}_{\mathrm{ISPP}}^{C}$, in contrast with the two outer branches $\mathsf{M}_{\mathrm{ISPP}}^{U}$ and $\mathsf{M}_{\mathrm{ISPP}}^{L}$, contains practically only one of the plasmonic components. This component coincides with the $I_{\mathrm{SPP}}^{\mathsf{C}}$ ($I_{\mathrm{SPP}}^{\mathsf{B}}$) mode in the case of the C (B) type structure. It means that the visibility of the peak corresponding the $\mathsf{M}_{\mathrm{ISPP}}^{C}$ branch should be much better in the case of the C type structure than in the B type structure, even when the condition $\omega_I = \omega_{\mathrm{IT}}$ is not well fulfilled. This prediction seems to be qualitatively consistent with the exact numerical results (see Figs. 13 and 14) obtained employing the transfer matrix approach. Note, however, that in our structures only the peak associated with the $\mathsf{M}_{\mathrm{ISPP}}^{U}$ and $\mathsf{M}_{\mathrm{ISPP}}^{C}$ branches can be observed. (The $\mathsf{M}_{\mathrm{ISPP}}^{L}$ branch is located below the backed/spacer medium light line.) As mentioned, in Fig. 13 the peaks positioned at $\hbar\omega$ close to 72 and 65.5 meV can be associated with the branches $\mathsf{M}_{\mathrm{ISPP}}^{U}$ and $\mathsf{M}_{\mathrm{ISPP}}^{C}$, supported by the degenerate structure ($\bar{\omega}_{p,\mathrm{mirr}}^{\mathrm{surf}} = \bar{\omega}_{\mathrm{IT}} = 0.5$). It is clearly seen that, although in the above structure the condition $\bar{\omega}_{\mathrm{IT}} \cong \bar{\omega}_I$ is not fulfilled, the relative heights of the peaks (associated with $\mathsf{M}_{\mathrm{ISPP}}^{U}$ and $\mathsf{M}_{\mathrm{ISPP}}^{C}$ branches) are different when the MQW is located at the coupling mirror (the gray dashed curve) and back mirror (the gray solid curve). We have checked numerically (results are not presented) that in agreement with the modified three-oscillator model, the above-mentioned difference dramatically increases when $\bar{\omega}_{\mathrm{IT}}$ approaches to $\bar{\omega}_I$ (≈ 0.36 at $\bar{k}_x \cong 0.5$). Simulation shows that, in the case of the B type structure, the peak associated with the $\mathsf{M}_{\mathrm{ISPP}}^{C}$ branch practically vanishes if $\hbar\omega_{\mathrm{IT}}$ ($\bar{\omega}_{\mathrm{IT}}$) is close to 50 meV (0.36). It is also worth noting that the visibility of the peak associated with the in-gap polaritons is enhanced by the location of the MQW near the coupling mirror. (See the behavior of the gray solid and dashed curves in Fig. 14 at $\hbar\omega \lesssim \hbar\omega_{\mathrm{IT}} = 69.3$ meV.)

[1] D. Dini, R. Kohler, A. Tredicucci, G. Biasiol, and L. Sorba, Phys. Rev. Lett. **90**, 116401 (2003).

[2] P. Jouy, A. Vasanelli, Y. Todorov, L. Sapienza, R. Colombelli, U. Gennser, and C. Sirtori, Phys. Rev. B **82**, 045322 (2010).

[3] R. Colombelli and J.-M. Manceau, Phys. Rev. X **5**, 011031 (2015).

[4] Y. Todorov, A. M. Andrews, I. Sagnes, R. Colombelli, P. Klang, G. Strasser, and C. Sirtori, Phys. Rev. Lett. **102**, 186402 (2009).

[5] Y. Todorov and C. Sirtori, Phys. Rev. B **85**, 045304 (2012).

[6] B. Askenazi, A. Vasanelli, A. Delteil, Y. Todorov, L. C. Andreani, G. Beaudoin, I. Sagnes, and C. Sirtori, New J. Phys. **16**, 043029 (2014).

[7] J.-M. Manceau, S. Zanotto, T. Ongarello, L. Sorba, A. Tredicucci, G. Biasol, and R. Colombelli, Appl. Phys. Lett. **105**, 081105 (2014); J.-M. Manceau, G. Biasiol, N. L. Tran, I. Carusotto, and R. Colombelli, Phys. Rev. B **96**, 235301 (2017).

[8] E. Dupont, H. C. Liu, A. J. SpringThorpe, W. Lai, and M. Extavour, Phys. Rev. B **68**, 245320 (2003).

[9] E. Dupont, J. A. Gupta, and H. C. Liu, Phys. Rev. B **75**, 205325 (2007).

[10] A. A. Bogdanov and R. A. Suris, Phys. Rev. B **83**, 125316 (2011).

[11] S. A. Maier, *Plasmonics: Fundamentals and Applications* (Springer, New York, 2007).

[12] Y. Kurokawa and H. T. Miyazaki, Phys. Rev. B **75**, 035411 (2007).

[13] F. Intravaia, C. Henkel, and A. Lambrecht, Phys. Rev. A **76**, 033820 (2007).

[14] S. E. Kocabas, G. Veronis, D. A. B. Miller, and S. Fan, Phys. Rev. B **79**, 035120 (2009).

[15] M. Bordag, Phys. Rev. D **85**, 025005 (2012).

[16] V. V. Nesterenko and I. G. Pirozhenko, Phys. Rev. A **86**, 052503 (2012).

[17] M. Skorobogatiy, *Nanostructured and Subwavelength Waveguides: Fundamentals and Applications* (Wiley, Chichester, 2012).

[18] M. Litinskaya and V. M. Agranovich, J. Phys.: Condens. Matter **24**, 015302 (2012).

[19] H. Shin, M. F. Yanik, S. Fan, R. Zia, and M. L. Brogersma, Appl. Phys. Lett. **84**, 4421 (2004).

[20] J. S. Q. Liu and M. L. Brongesma, Appl. Phys. Lett. **90**, 091116 (2007).

[21] J. Feng, T. Okamoto, J. Simonen, and S. Kawata, Appl. Phys. Lett. **90**, 081106 (2007).

[22] H. J. Lezec, J. A. Dionne, and H. A. Atwater, Science **316**, 430 (2007).

[23] S. Kalusniak, S. Sadofev, and F. Henneberger, Opt. Express **23**, 30079 (2015).

[24] S. Law, C. Roberts, T. Kilpatrick, L. Yu, T. Ribaudo, E. A. Shaner, V. Podolskiy, and D. Wasserman, Phys. Rev. Lett. **112**, 017401 (2014).

[25] S. Lan, L. Kang, D. T. Schoen, S. P. Rodrigues, Y. Cui, M. L. Brongersma, and W. Cai, Nat. Mater. **14**, 807 (2015).

[26] J. Park, K.-Y. Kim, L.-M. Lee, H. Na, S.-Y. Lee, and B. Lee, Opt. Express **18**, 598 (2010).

[27] E. Feigenbaum, N. Kaminski, and M. Orenstein, Opt. Express **17**, 18934 (2009).

[28] A. Reza, M. M. Dignam, and Hughes, Nature (London) **455**, E10 (2008).

[29] A. Archambault, M. Besbes, and J.-J. Greffet, Phys. Rev. Lett. **109**, 097405 (2012).

[30] A. Ciattoni, A. Marini, C. Rizza, M. Scalora, and F. Biancalana, Phys. Rev. A **87**, 053853 (2013).

[31] K. L. Tsakmakidis, T. W. Pickering, J. M. Hamm, A. F. Page, and O. Hess, Phys. Rev. Lett. **112**, 167401 (2014).

[32] S. Wuestner, T. Pickering, J. M. Hamm, A. F. Page, A. Pusch, and O. Hess, Faraday Discuss. **178**, 307 (2015); J. Baumberg, M. Noginov, J. Aizpurua, K. Lin, T. Ebbesen, A. A. Kornyshev, R. Sapienza, N. van Hulst, S. Kotni, F. J. García de Abajo, P. Ginzburg, O. Hess, M. Brongersma, and S. Bozhevolnyi, *ibid.* **178**, 325 (2015).

[33] T. Pickering, J. M. Hamm, A. Freddie, S. Wustner, and O. Hess, Nat. Commun. **5**, 4972 (2014).

[34] M. B. Pande and S. Dutta Gupta, Opt. Soc. Am. B **9**, 2265 (1992).

[35] S. Hayashi, Y. Ishigaki, and M. Fujii, Phys. Rev. B **86**, 045408 (2012).

[36] S. Kena-Cohen, S. Mayer, and D. D. Bradley, Adv. Opt. Mater. **1**, 827 (2013).

[37] M. Załużny and W. Zietkowski, Phys. Rev. B **88**, 195408 (2013).

[38] M. Załużny and W. Zietkowski, Phys. Rev. B **80**, 245301 (2009).

[39] P. Shekhar and Z. Jacob, Phys. Rev. B **90**, 045313 (2014).

[40] S. Campione, I. Brener, and F. Marquier, Phys. Rev. B **91**, 121408 (2015).

[41] S. Campione, S. Liu, A. Benz, J. F. Klem, M. B. Sinclair, and I. Brener, Phys. Rev. Appl. **4**, 044011 (2015).

[42] A. Armitage, M. S. Skolnick, A. V. Kavokin, D. M. Whittaker, V. N. Astratov, G. A. Gehring, and J. S. Roberts, Phys. Rev. B **58**, 15367 (1998).

[43] B. Liu, P. Rai, J. Grezmak, R. J. Twieg, and K. D. Singer, Phys. Rev. B **92**, 155301 (2015).

[44] N. M. Sundaresan, Y. Liu, D. Sadri, L. J. Szőcs, D. L. Underwood, M. Malekakhlagh, H. E. Türeci, and A. A. Houck, Phys. Rev. X **5**, 021035 (2015).

[45] C. Ouellet-Plamondon, G. Sallen, F. Jabeen, D. Y. Oberli, and B. Deveaud, Phys. Rev. B **92**, 075313 (2015); C. Ouellet-Plamondon, Ph.D. thesis, EPFL, Lausanne, 2017.

[46] A. Zheng, G. Zhang, H. Chen, T. Mei, and J. Liu, Sci. Rep. **7**, 14001 (2017).

[47] M. Załużny and C. Nalewajko, Phys. Rev. B **59**, 13043 (1999).

[48] D. Wei, C. Harrison, C. C. Bomberger, J. Zhang, J. Zide, and S. Law, Opt. Express **24**, 8735 (2016).

[49] R. C. Newman, Mater. Sci. Eng., B **66**, 39 (1999).

[50] Y. Ch. Jun, J. Reno, T. Ribaudo, E. Shaner, J.-J. Greffet, S. Vassant, F. Marquier, M. Sinclar, and I. Brener, Nano Lett. **13**, 5391 (2013).

[51] T. Taliercio, V. N. Guilengui, L. Cerutti, E. Tournie, and J.-J. Greffet, Opt. Express **22**, 24294 (2014).

[52] A. J. Hoffman, L. Alekseyev, S. S. Howard, K. J. Franz, D. Wasserman, V. A. Podolskiy, E. E. Narimanov, D. L. Sivco, and C. Gmachl, Nat. Mater. **6**, 946 (2007); K. Feng, G. Harden, D. L. Sivco, and A. J. Hoffman, ACS Photonics **4**, 1621 (2017).

[53] F. Omeis, R. Smaali, F. Gonzalez-Posada, L. Cerutti, T. Taliercio, and E. Centeno, Appl. Phys. Lett. **111**, 121108 (2017).

[54] H. M. K. Wong and A. S. Helmy, J. Opt. Soc. Am. B **30**, 1000 (2013).

[55] W. Zietkowski and M. Załużny, J. Appl. Phys. **96**, 6029 (2004).

[56] S. Zanotto, Ph.D. thesis, Scuola Normale Superiore, 2014.

[57] Y. Todorov, Phys. Rev. B **89**, 075115 (2014).

[58] Y. C. Jun, R. D. Kekatpure, J. S. White, and M. L. Brongersma, Phys. Rev. B **78**, 153111 (2008).

[59] S. Zanotto, R. Degl'Innocent, L. Sorba, A. Tredicucci, and G. Biasiol, Phys. Rev. B **85**, 035307 (2012).

[60] A. González-Tudela, P. A. Huidobro, L. Martin-Moreno, C. Tejedor, and F. J. Garcia-Vidal, Phys. Rev. Lett. **110**, 126801 (2013).

[61] M. Litinskaya and V. M. Agranovich, J. Phys.: Condens. Matter **21**, 415301 (2009).

[62] Ch. Feuillet-Palma, Y. Todorov, R. Steed, A. Vasanelli, G. Biasol, L. Sorba, and C. Sirtori, Opt. Express **20**, 29121 (2012).

[63] A. Archambault, F. Marquier, J.-J. Greffet, and Ch. Arnold, Phys. Rev. B **82**, 035411 (2010).

[64] S.-W. Chang and S. L. Chuang, Opt. Lett. **34**, 91 (2009).

[65] F. Alpeggini and L. Andreani, Plasmonics **9**, 965 (2014).

[66] F. D. Nunes, T. C. Vasconcelos, M. T. Bezerra, and J. Weiner, J. Opt. Soc. Am. B **28**, 1544 (2011).

[67] Q. Gu, B. Slutsky, F. Vallini, J. S. T. Smalley, M. P. Nezhad, N. C. Frateschi, and Y. Fainman, Opt. Express **21**, 15603 (2013).

[68] J. E. Sipe, J. Opt. A **11**, 114006 (2009).

[69] A. Raman and S. Fan, Phys. Rev. Lett. **104**, 087401 (2010); Phys. Rev. B **83**, 205131 (2011).

[70] B. Xi, M. Qiu, S. Xiao, H. Xu, and L. Zhou, Phys. Rev. B **89**, 035110 (2014).

[71] K. Kim and D. Stroud, Opt. Express **21**, 19834 (2013).

[72] K. Zhang, W.-B. Shi, D. Wang, Y. Xu, R.-W. Peng, R.-H. Fan, Q.-J. Wang, and M. Wang, Appl. Phys. Lett. **108**, 193111 (2016).

[73] M. Załużny, W. Zietkowski, and C. Nalewajko, Phys. Rev. B **65**, 235409 (2002).

[74] N. C. Chen, C. Y. Lu, Y. L. Huang, C. C. Liao, W. C. Ke, and B. R. Huang, J. Appl. Phys. **112**, 033111 (2012).

[75] K. Y. Kim, J. Opt. A **11**, 075003 (2009).

[76] D. Li, K. Du, S. Liang, W. Zhang, and T. Mei, Opt. Express **24**, 22432 (2016).

[77] A. A. Sayem, M. R. C. Mahdy, D. N. Hassan, and M. A. Matin, in *Proceedings of the International Conference on Electrical and Computer Engineering* (IEEE, Piscataway, NJ, 2014), pp. 230–233.

[78] H. Xu, L. Wu, X. Dai, Y. Gao, and Y. Xiang, Optics **127**, 9640 (2016).

[79] G. Gonzalez de la Cruz, Solid State Commun. **262**, 11 (2017).

[80] M. Załużny and C. Nalewajko, J. Appl. Phys. **107**, 123106 (2010).

[81] G. S. Agrawal and S. D. Gupta, Opt. Lett. **27**, 1205 (2002).